ESA UNCLASSIFIED – For Official Use

DOCUMENT

MarcoPolo-R
Payload Definition Document
PDD

Prepared by	**MarcoPolo-R Study Team**
Reference	**SRE-PA/2011.079**
Issue	**1.0**
Revision	
Date of Issue	**04/11/2011**
Status	**Draft**
Document Type	
Distribution	

European Space Agency
Agence spatiale européenne

APPROVAL

Title	
Issue 1.0	**Revision**
Author	**Date** 04/11/2011
Approved by	**Date**

CHANGE LOG

Reason for change	Issue	Revision	Date

CHANGE RECORD

Issue 1.0	Revision		
Reason for change	**Date**	**Pages**	**Paragraph(s)**

Table of contents:

1 INTRODUCTION

2 ACRONYMS

AD	Applicable Document
APS	Active Pixel Sensor
APXS	Alpha Particle X-ray Spectrometer
AU	Astronomical Unit
BELA	BepiColombo Laser Altimeter
CPEM	Charged Particle Environment Monitor
CSU	Common Support Unit
CUC	Close-Up Camera
DTM	Digital Terrain Model
EGLO	Extended Monitoring
ESA	European Space Agency
FAR	Formation Flying
FEE	Front End Electronics
FM	Flight Model
FOV	Field of View
GLO	Global Characterisation
LIBS	Laser Induced Breakdown Spectroscopy
LOC	Local Characterisation
midIR	mid infrared
MPCS	Marco Polo Camera System
MRD	Mission Requirement Document
MTF	Modulated Transfer Function
N/A	Not Applicable
NAC	Narrow Angle Camera
NAHRIC	Narrow Angle – High Resolution Camera
NEA	Near Earth Asteroid
NEO	Near Earth Object
N/A	Not Applicable
N/K	not known
NPA	Neutral Particle Analyser
PSF	Point Spread Function
QE	Quantum Efficiency
RD	Reference Document
RSE	Radio Science Experiment
SAM	Sampling and sample context measurements
SRD	Science Requirements Document
SST	Study Science Team
TBC	To Be Confirmed
TBD	To Be Determined
TMA	Three Mirror Anastagmatic
TRL	Technology Readiness Level
WAC	Wide Angle Camera
XRF	X-Ray Fluorescence

3 LIST OF FIGURES AND TABLES

3.1 List of figures

3.2 List of tables

4 APPLICABLE AND REFERENCE DOCUMENTS

[AD1] **MPR-RSSD-RS-001** Science Requirements Document
[AD2] **SRE-PA/2011.076** MarcoPolo-R Mission Requirements Document (MRD)
[AD3] **SRE-PA/2011.077** MarcoPolo-R Mission Environment Document
[AD4] **SRE-PA/2011.078** MarcoPolo-R – Assessment of Planetary Protection issues

5 CONTACT PERSONS

6 PAYLOAD OVERVIEW AND SUMMARY TABLES

6.1 Baseline payload complement

The main scientific goal of this mission is to return a sample from a primitive Near Earth Object (NEO) to Earth. However, a dedicated suite of scientific instruments is required to identify the best landing sites, collect context information and for an overall description of the NEO and its environment.
The proposed model payload consists of the following elements,

- **Wide Angle Camera**
- **Narrow Angle Camera**
- **Close-up Camera**
- **Visible/Near Infrared Spectrometer**
- **Mid Infrared Spectrometer**
- **Radio Science Experiment**

- **Neutral Particle Analyzer**

These were defined by the Science Team in order to meet the science requirements defined in [AD1]. It is important to note that the primary set of instruments (core payload complement) helps fulfil the science requirements defined in [AD1] as “shall” requirements while the additional scientific objectives (defined as “should” in [AD1]) are being addressed by a set of complementary instruments defined in chapter 8.8 .

Table 1Summary of resource budgets per instrument of the baseline payload complement

	WAC	**NAC**	**Close up imager**	**VisNIR**	**MidIR**	**RSE[##]**	**NPA**	**Σ**
Overall TRL[#]	4	4	3	5	4-5	9	4 - 5	
Units	1 (+1 CSU)	1 (+1 CSU)	1 (+1 CSU)	2	1	1	1	
Interface to S/C								
accommodation	observ. plat.	observ. platform	S/C bottom	observ. platform	observ. platform	comms	obs. platform	
mechanical	flat mounted	flat mounted	S/C body	flat mounted	flat mounted	-	Flat mounted	
electrical	28 V regulated	28 V regulated	28 V regulated	28 V regulated	28 Vregulated	-	28 V regulated	
data	Spacewire	Spacewire	SpaceWire	Spacewire	CAN bus	-	CAN bus	
thermal	radiator	radiator	Radiator	radiator	radiator	-	-	
Weight [kg][###]	2.0	6.0 + 2.9 (CSU)	0.82	3.6	3.0	-	2.2	**20.52**
Volume [mm]	237x172x115	520x380x197 250x170x120 (CSU)	364x78x68	260x128x84 150x180x65	160x220x370	-	200x200x100	
Power [W]								
peak	11.5	13.5	12.5	18	3.5	-	11.5	
observation	11.5[*]	13.5[*]	12.5[*]	18	2	-	11.5	**45.0[**]**
standby	5.0 (CSU only)	5.0 (CSU only)	5.0 (CSU only)	7.0 (cooler)	1	-	7.0	
Temperature ops /non-ops [°C]	0 / -27 -60/ -40 det.	0 to -27 / -60 to -40 detector	-0/+30 -60/+40	-123°C (detector)/	<-10	tbd	-20/+40 -40/+50	
Data product								
single	67.0 Mbit	67.0 Mbit	67.0 Mbit	0.45 Mbit	360 Mbit[@]	-	0.72 kbit	
Compression	1.8	1.8	1.8	3-10	2.5	n/a	2	
Pointing	nadir	nadir	Sampling site	nadir[@@]	nadir	-	nadir	
absolute error	0.1 mrad	0.1 mrad	fixed			better than 0.1 x 3dB beam width	10 mRad	
relative error (stability)	0.2 mrad/s	0.03 mrad/s	0.1	0.12 mrad	0.1 mrad (over 7 seconds)	see instrument description	object within field of view	
Field of view [deg]	11.2	1.7					5x30	

[#]The TRL estimate is based on the information provided by external institutions. More detailed TRL assessment can be found in some of the individual instrument chapters.
[##]The resources of the RSE are allocated in the communication system of the spacecraft
[###] **no maturity margin included**
[*]value includes CSU
[**] Only one camera working at the time. NAC is included in the sum. CUC operations only during the sample procedure on while all other payload is switched off.
[@] 1 surface map whole body
[@@] aligned with NAC within an accuracy of 0.12 mrad

Table 2 Timeline of observations for MarcoPolo-R

	days	distance	comments
Global mapping / far global characterization	21	5 km	Distance as for Marco Polo (no risk of microparticles), duration = average Rosetta/Marco Polo
Close observation phase/ global characterization	14	2 km tbc	Duration as Marco Polo (Rosetta 23 days, but no local characterization)
Detailed gravity mapping	0	200 m	No terminator orbit operations for Marco Polo R
Local characterization	35	100 m tbc	As Marco Polo
Landing	35	0	Marco Polo duration (70 days) was sized for 5 landing attempts, to be reduced, Rosetta: 27 days
Additional science	0	-	TBD as time available
Asteroid escape preparation	7	-	As per Marco Polo, SEP impact TBD

Table 2is subject of further detailed analysis during the course of study. However, it has to be noted that the observation duration is ***considerably*** lower than in the case of the Marco Polo scenario.

7 MISSION PROFILE AND SCIENCE OPERATIONS - SUMMARY

8 DESCRIPTION OF BASELINE INSTRUMENTS

8.1 Marco Polo Camera System MPCS – Wide Angle Camera WAC

8.1.1 Introduction

This section describes a wide angle camera WAC compatible with the Marco Polo mission requirements. Scientific issues that can be addressed with this experiment are also identified.

8.1.2 Scientific Goals and Performance Requirements

The main scientific objective of the WAC can be summarized in the following sentence (taken from the science requirements document):

GR-030: A shape model of the NEA shall be obtained with an accuracy of typically 1 m in height and spatial resolution with respect to the centre of mass, in both illuminated and unilluminated regions.

The shape can be obtained if the entire asteroid is included in one WAC image while the spacecraft is in a distant orbit for global characterisation of the target. The shape and mass provide information on the bulk density of the body. WAC images are also used for the determination of the rotation motion of the body (period, axis, state), to provide the larger surface context for NAC fields and to find the asteroid in the stellar field when the payload will be switched on. Its wide field is suitable for search of satellites around the main target and its f ratio brings advantages for the identification of low surface brightness structures, for instance during limb sounding for activity. Last, but not least, the WAC may also be utilized for navigation purposes, in particular during the approach phase to the NEO.

8.1.3 Description

The WAC is a small aperture camera for the visible wavelength range providing wide angle low resolution images of the target (or other fields). Single bandpass imaging is sufficient for the WAC applications.

8.1.3.1 Instrument concept

The WAC is a compact dioptric design with a 105 mm focal length and 16mm aperture. The f ratio is kept as slow as possible, compatible with the scientific and the mechanical constraints, in order to have a large field of view and high sensitivity. The WAC design shall

perform imaging of the full body silhouette of an object like 1996 FG3 from a distance of about 5km. It is mandatory to achieve very high performance in the modulated transfer function (MTF) of the WAC in order to allow surface imaging at high contrast.
The lenses for this camera are small, simple, and effective and the fewest number of lens elements is used. All optical surfaces are spherical or flat. A modified double Gauss design is adopted paying attention to lateral and axial color balancing and to keep distortion as low as possible.

The same detector system (active pixel sensor (APS) detector, 2048 x 2048 pixels, 10 x 10 µm pixel size, front-end electronics FEE) as used for the NAC is also used for the WAC. Sensor and FEE are attached to the camera structure. Refocusing of the camera is not foreseen. An instrument baffling suppresses straylight.

The instrument is complemented by the common support unit CSU that contains the power control unit PCU and the command and data processing unit CDPU. The CSU serves all three science cameras (WAC, NAC, CUC) onboard MarcoPolo in providing power and handling the command and data processing of the imaging systems and has built-in redundancy.

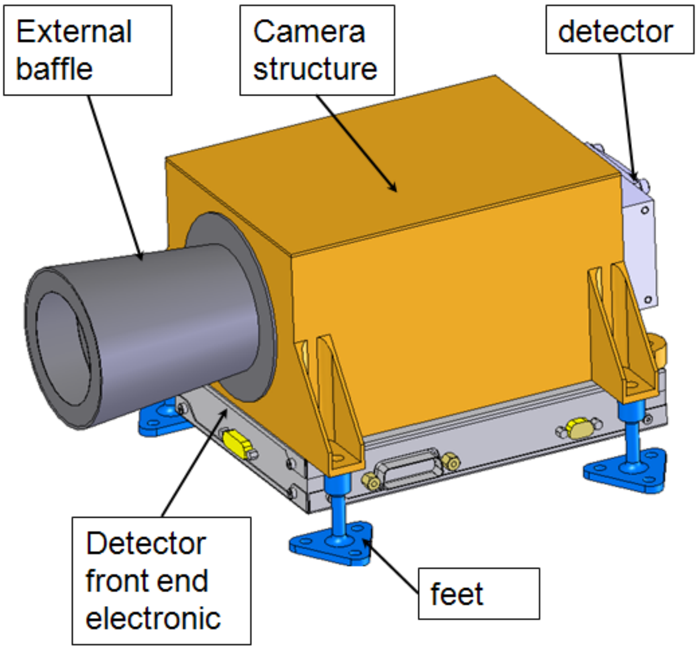

Figure 1 MPCS WAC - Mechanical structure. Upper panel: schematics of the mechanical structure; lower panel: detailed views.

8.1.3.2 Operation requirements

The WAC will be used in framing mode

- nadir pointing for body shape imaging and rotation monitoring
- limb pointing for special applications like shape model details and activity search

- any pointing direction for in-flight calibrations and special applications at the target (satellite search) and for navigation purposes

Full orbit operations must be possible. Default operation is by timeline; in exceptional cases (commissioning, in-flight problems, special science and navigation applications) commanding and data transmission in interactive mode may be required.

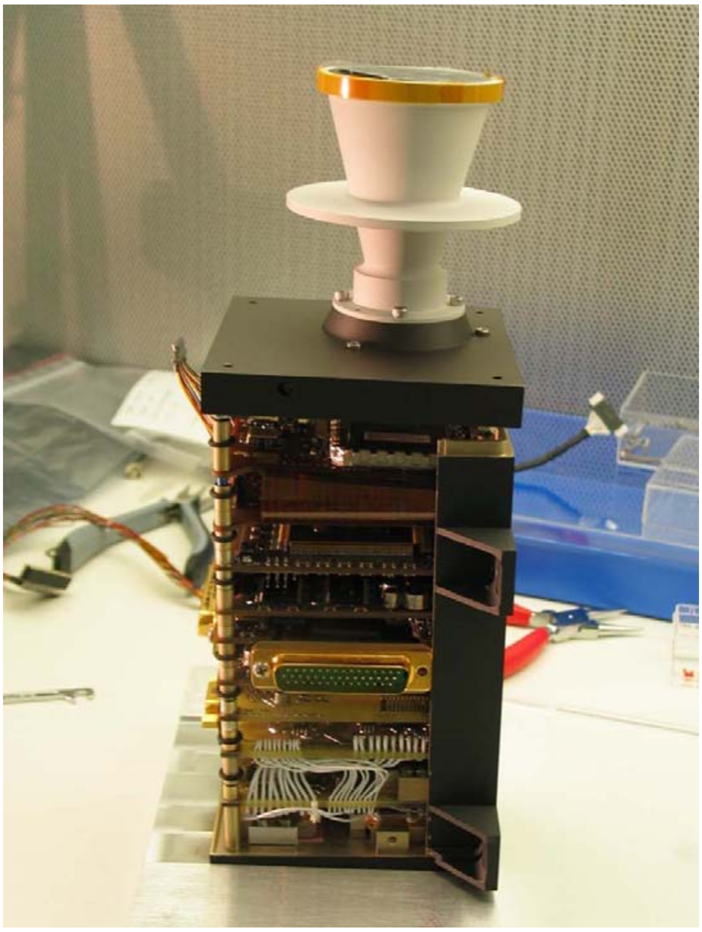

Figure 2 An example for a WAC - the VMC camera onboard VenusExpress

8.1.3.3 Interfaces and physical resource requirements

The WAC camera is fixed mounted pointing into nadir direction. The CSU is mounted separately from the WAC (and NAC, CUC) and is connected with the camera and the spacecraft through Spacewire and power lines. A close arrangement between the WAC, NAC, CUC and CSU is advantageous. Proper temperature range of detector system and opto-mechanics is critical for camera operations and performance quality. Active control may be required.

8.1.3.4 Calibration

The ground calibration activity shall provide the characterisation of the spectral, geometric, radiometric and linearity properties of the camera. The measurements have to be realized on each subsystem (h/w units to be integrated in the WAC).

The WAC in-flight calibration will be based on the observation of selected star fields in order to verify:

- PSF
- Optical axis pointing direction
- Image distortion
- Spectral and radiometric calibration

Furthermore, the WAC and the NAC have to follow common activities as:

- Co-alignment of the bore-sights of each camera with respect to the nadir pointing axis
- Cross spatial registration (relative spatial offsets for each camera)
- Radiometric cross-calibration

The relative boresight alignment of the WAC may also be of interest with respect to other instruments (laser altimeter, spectrometer).

8.1.3.5 Cleanliness, planetary protection and pre-launch activities

Normal requirements for cleanliness and pre-launch activities as typical for visible cameras used for space exploration will be applied. Since the instrument is not meant to reach the surface, planetary protection issues are not applicable (except the whole spacecraft crashes or remains in an unintended way on the surface of the NEO).

8.1.3.6 Critical points

The WAC may not deliver properly focused images of the body surface during the close approach phase to the NEO. Dust contamination by thrusters firing during landing and ascent may require the implementation of a dust protection door for the WAC.

8.1.3.7 Heritage

VMC in VenusExpress, SIMBIOSYS in BepiColombo.

Table 3 Summary table of WAC instrument (Note: WAC operations will require operations of the common support unit CSU for the MarcoPolo camera system consisting of WAC, NAC, and CUC)

Parameter	*Unit*	*Value / Description*	*Remarks*
Reference P/L	n/a	SIMBIOSYS, VMC	
Type of optics	n/a	Dioptric	Unobstructed
Type of camera	n/a	Wide angle camera	
OPTICS			
Pupil diameter	mm	16	
Focal length	mm	105	
F ratio	n/a	6.5	Diffraction limited at 600 nm
Field of view	°	11 x11	
Pixel scale	''/px	19.5	
Spectral range	nm	400-950	
Filters		1	Panchromatic or medium wide, laser spot wavelength included is TBD
DETECTOR			
Type of detector	n/a	Si PIN-CMOS	Hybrid
Pixel size	µm x µm	10 x 10	
Pixel number		2048x2048	
Exposure time	ms	≤2	
Read out time	µsec/px	0.2	~0.85s read-out time per full frame
Full well capacity	e^-	>120000	
A/D conversion	Bit	14	Final raw data: 16 Bit
Operating Temperature		0°C -- +27°C	
CONFIGURATION / LAYOUT			
Units	#	1	Plus shared CSU
Preferred location for sensor	n/a	Focal plane	
Preferred location for electr.	n/a	compact arrangement	
Excitation sources	#	n/a	
Strength of sources	mCi	n/a	
PHYSICAL			
Mass, total (no margins)	g	2000	WAC (incl. opto-mechanics, detector, FEE, housing, baffling, internal harness)

Dimensions (no margins)	mm^3	273x172x115	WAC (incl. opto-mechanics, detector, FEE, housing, baffling, internal harness)
Sample area	mm^2	50 x 50	assumed
POWER			
Average (no margins)	W	11.5	WAC detector+CSU
Peak	W	11.5	
DATA RATE / VOLUME			
Average tm rate	MBit/s	68	Maximum
Data volume per image	MBit	67	(excl. header infos)
Data volume total (raw data volume, uncompressed)	GBit		
POINTING			
Pointing	µrad	100	
Pointing accuracy	µrad/s	200	
THERMAL			
Temperature ranges op. Sensor Head and electronics board	°C	0 -- +27	
Temp. ranges op. Deployment-device		n/a	
Temperature ranges Non-op	°C	-60 -- +40	
Temp. ranges non-op. deployment-device		n/a	
Temperature stability	°C	1	
CONTAMINATION			
EMC requirements	power supply	TBD	ESA EMC specs to be applied
DC magnetic	n/a	n/a	
Chemical requirements	n/a	n/a	
SUPPORT ITEMS			

Deployment system	n/a	n/a	
Covers, Shutters	n/a	n/a	Need for aperture door is TBD by dust contamination analysis

8.2 Marco Polo Camera System MPCS – Narrow Angle Camera NAC

8.2.1 Introduction

This section describes a narrow angle camera compatible with the Marco Polo mission requirements. Scientific issues that can be addressed with this experiment are also identified.

8.2.2 Scientific Goals and Performance Requirements

The following requirements are cited from the Science Requirements Document as reference for the expected scientific performance of this instrument:

LR-010: A representative area within the expected landing area ellipse (goal: entire ellipse) shall be imaged in the visible in at least three colour filters, with a spatial resolution of the order of millimetres.

GR-010: The complete surface of the NEA shall be imaged in at least 3 different colours, in the visible range with a spatial resolution of the order of decimetres, and with local solar elevation angle between 30 and 60° (Note: it is acknowledged that depending on the rotation axis of the asteroid there may be areas which cannot be imaged due to illumination constraints).
GR-030: A shape model of the NEA shall be obtained with an accuracy of typically 1 m in height and spatial resolution with respect to the centre of mass, in both illuminated and unilluminated regions.

High spatial resolution images will be necessary to carefully analyze the morphology and topography of the NEO surface. Thanks to the high spatial resolution observations it will be possible to identify landing sites that are suitable (from the scientific and operations points of view).for sample acquisitions.

High spatial resolution images will be of paramount importance for the overall target body characterization in terms of:

• surface topography and distribution of morphological features (e.g., boulders, craters, fractures)
• generation of a Digital Terrain Model (DTM) of some regions
• analysis about NEO fragmentation/accretion history and evolution
• bulk composition of the body (size, shape, rotational properties)
• overall characteristics like orbit, rotation, size, shape, mass, gravity and density

NAC imaging may also be needed for complementary details of the shape model obtained mostly through WAC imaging and for a close characterization of any satellite body that might be known to exist or that might be discovered by the mission around the main target.

Furthermore, high spatial resolution images shall be also important for the:

• spacecraft navigation
• exploration of mineralogical and chemical compositions.

8.2.3 Description

Primitive asteroids are intrinsically dark objects; hence, for the performance estimation of the instrument an average albedo of 0.06 is assumed. It also implies that the surface features have typically a low contrast. The low albedo makes it difficult to obtain high contrast images that are necessary to well study the regolith properties. A high contrast image can be obtained only if the optical contrast performance of the camera, including the residual diffraction contribution, is very high.

Optical designs with central obscuration are well known for a loss of contrast in extended object imaging and for straylight problems. Therefore, for the NAC, an unobstructed and unvignetted optical design concept is very much preferred. Moreover, one of the main scientific objectives of the NAC is the generation of the Digital Terrain Model (DTM) of specific regions, which is based on the matching of the windows obtained in different images of the same areas. The central obstruction reduces the matching capabilities and, consequently, the vertical accuracy, since it degrades the point spread function (PSF) sharpness and decreases the modulation transfer function (MTF).

8.2.3.1 Instrument concept

The NAC optical design is based on an off-axis TMA (three mirror anastigmatic) configuration which follows the heritage of the OSIRIS cameras for the Rosetta mission, that are working in-flight, very well satisfying the original specifications.

The NAC design is based on a focal ratio of 8 and a focal length of 660 mm, in order to provide the spatial resolution set in the scientific requirements (order of mm at 200m distance). The diffraction limit has been calculated at 650 nm which is the middle of the spectral range coverage requested, in order to have an encircled energy greater than 70% all over the field of view (FoV) and in the entire spectral range of interest for the camera. The NAC layout guarantees good aberration balancing over the full FoV of the instrument, an MTF greater than 52% and distortion less than 1.5%.

A minimum of 3 to up to 8 filters can be applied for NAC imaging. Filter band widths can be as narrow as 5-10nm. The filters will be directly and permanently applied in front of the detector.

The requirement to observe very close to the surface, i.e. at 200 m above the surface, is very demanding in terms of focus depth, which is not possible to satisfy without introducing a mechanism moving – at least - one optical element in the camera. The focusing mechanism of the NAC allows sharp imaging between 150m and infinity. Furthermore, the focal plane position is sensitive to very small variation of the distance of surface elements which requires the usage of focus distance information through an appropriate sensing device or through a-priori knowledge (options are: laser altimeter, NAC focusing routine, orbit and shape information). An instrument baffling suppresses straylight.

The NAC is designed around a detector of 2048 x 2048 pixels with pixel size of 10 μm to guarantee a pixel scale of 3 cm over the field of view of 1.7°x1.7° when imaging the surface at 2 km distance. An array solution is preferred over linear detectors in order to allow snapshot image acquisition, which appears less critical with respect to requirements on pointing and stability, and reducing the number of images for a surface mosaic. The imaging sensor is based on a Hybrid Active Pixel Sensor (APS) that uses CMOS readout technology. Its characteristics/capabilities of low power consumption, high radiation tolerance and very high Quantum Efficiency (QE) ensure a high performance of the camera system, even for short exposure times of the order of milliseconds, as it may be required in the MarcoPolo mission. Sensor and front-end electronics (FEE) are attached to the camera structure.

The instrument is complemented by the common support unit CSU that contains the power control unit PCU and the command and data processing unit CDPU. The CSU serves all three science cameras (WAC, NAC, CUC) onboard MarcoPolo in providing power and handling the command and data processing of the imaging systems and has built-in redundancy.

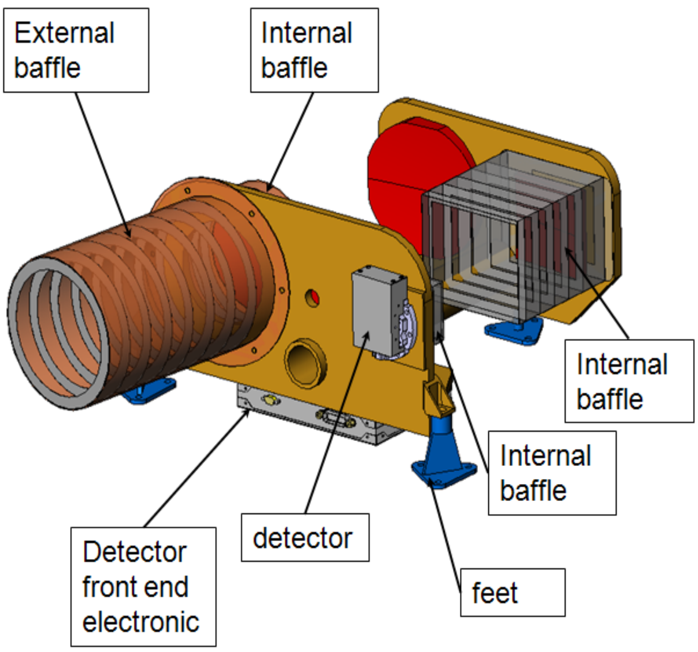

Figure 3 MPCS NAC: The mechanical structure and the focusing device. Top panel: Schematics; Lower panels: Detailed drawings of the NAC camera structure.

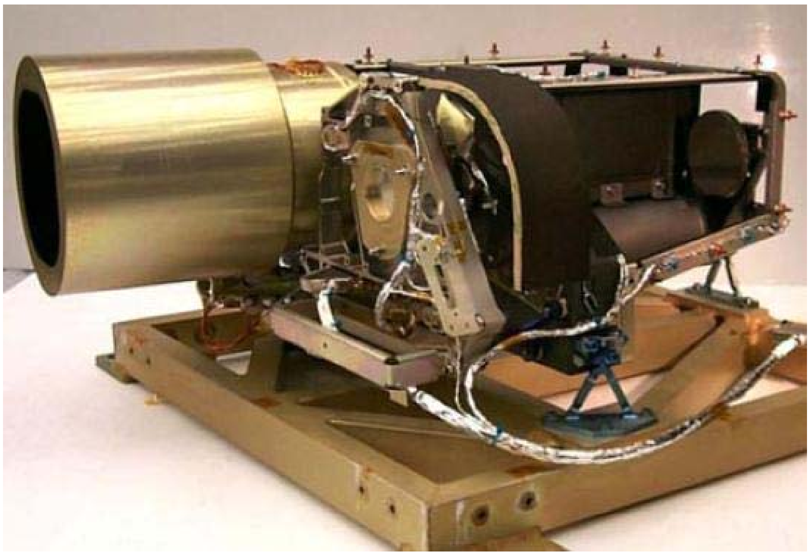

Figure 4 Example for a NAC – the Osiris NAC onboard the Rosetta mission

8.2.3.2 Operation requirements

The NAC will be used in special framing mode:

nadir pointing during global mapping of the target
nadir and off-nadir pointing (0-60 deg) for the TDM application of the target
limb pointing for special applications like shape model details and activity search
any pointing direction for in-flight calibrations and special applications at the target (satellite imaging)

Special framing mode implies that single image frames of the surface are taken, with individual segments of the image showing different parts of the surface through different filters.

Full orbit operations must be possible. Default operation is by timeline; in exceptional cases (commissioning, in-flight problems, special science and navigation applications) commanding and data transmission in interactive mode may be required.

For NAC focus information coordinated operations between NAC and laser altimeter may be required. Alternatively, a NAC focus sequence can be obtained or a-priori knowledge of the focusing distance from orbit and shape models is applied.

8.2.3.3 Interfaces and physical resource requirements

The NAC camera is fixed mounted pointing into nadir direction. The CSU is mounted separately from the NAC (and WAC, CUC) and is connected with the camera and the spacecraft through Spacewire and power lines. A close arrangement between the WAC, NAC, CUC and CSU is advantageous. Proper temperature range of detector system and opto-mechanics is critical for camera operations and performance quality. Active control may be required.

8.2.3.4 Calibration

The ground calibration activity shall provide the characterisation of the spectral, geometric, radiometric and linearity properties of the camera. The measurements have to be realized on each subsystem (h/w units to be integrated in the NAC).

The NAC in-flight calibration will be based on the observation of selected star fields in order to verify:
- PSF
- Optical axis pointing direction
- Image distortion
- Spectral and radiometric calibration

Furthermore the NAC and the WAC have to follow common activities as:

- Co-alignment of the bore-sights of each camera with respect to the nadir pointing axis
- Cross spatial registration (relative spatial offsets for each camera)
- Radiometric cross-calibration

The relative boresight alignment of the NAC may also of interest with respect to other instruments (spectrometer).

8.2.3.5 Cleanliness, planetary protection and pre-launch activities

Normal requirements for cleanliness and pre-launch activities as typical for visible cameras used for space exploration will be applied. Since the instrument is not meant to reach the surface, planetary protection issues are not applicable (except the whole spacecraft crashes or remains in an unintended way on the surface of the NEO).

8.2.3.6 Critical points

The NAC may not deliver properly focused images of the body surface very close to the surface of the object (150m or less). Dust contamination by thruster firings during landing and ascent may require the implementation of a dust protection door for the NAC.

8.2.3.7 Heritage

OSIRIS in the Rosetta mission and SIMBIOSYS in the BepiColombo mission.

Table 4 Summary table of NAC instrument (Note: NAC operations will require operations of the common support unit CSU for the MarcoPolo camera system consisting of WAC, NAC, and CUC)

Parameter	*Unit*	*Value / Description*	*Remarks*
Reference P/L	n/a	OSIRIS / Rosetta SIMBIOSYS / BepiColombo	

Type of optics	n/a	TMA (three-mirror anastigmatic design)	Unobstructed all-reflective
Type of camera	n/a	Narrow angle camera	
OPTICS			
Pupil diameter	mm	82.5	
Focal length	mm	660	
F ratio	n/a	8	Diffraction limited at 650 nm
Field of view	°	1.7 x 1.7	Global FoV for all filters together single filter FoV ~1.7 x 0.15-0.20
Pixel scale	''/px	3.1	
Spectral range	nm	400 - 950	
Filters	n/a	4-8	Minimum = 4, maximum = 8
FOCUSING MECHANISM			
Vertical motion	mm	10 +/- 0.001	
Horizontal motion	mm	100 +/- 0.004	
DETECTOR			
Type of detector	n/a	Si PIN-CMOS	Hybrid
Pixel size	µm x µm	10 x 10	
Pixel number		2048 x 2048	
Exposure time	ms	≤2	
Read out time	µsec/px	0.2	~0.85s read-out time per full frame
Full well capacity	e^-	>120000	
A/D conversion	Bit	14	final raw data: 16 Bit
Operating Temperature	°C	0°C -- +27°C	
CONFIGURATION / LAYOUT			
Units	#	1	Plus shared CSU
Preferred location for sensor	n/a	Focal plane	It's a must (not only preferred)
Preferred location for electr.	n/a	Compact arrangement	
PHYSICAL			
Mass, total (no margins)	g	6000	NAC (incl. opto-mechanics, detector, FEE, housing, baffling, internal harness)
Dimensions	mm^3	520x380x197	NAC (incl. opto-mechanics, detector,

(no margins)			FEE, housing, baffling, internal harness)
Sample area	mm²	50 x 50	assumed
POWER			
Average (no margins)	W	13.5	NAC focus mechanism NAC detector+CSU
Peak	W	13.5	
DATA RATE / VOLUME			
Average tm rate	MBit/s	68	Maximum
Data volume per image	MBit	67	
Data volume total (raw data volume, uncompressed)	GBit		
POINTING			
Pointing	µrad	15	
Pointing accuracy	µrad/s	30	
THERMAL			
Temperature ranges op. Sensor Head and electronics board	°C	0°C -- +27°C	
Temp. ranges op. Deployment-device	°C	n/a	
Temperature ranges Non-op	°C	-60°C -- +40°C	
Temp. ranges Non-op. Deployment-device	°C	n/a	
Temperature stability	°C	1	
CONTAMINATION			
EMC requirements	power supply	TBD	ESA EMC specs to be applied
DC magnetic	n/a	n/a	
Chemical requirements	n/a	n/a	
SUPPORT ITEMS			
Deployment system	n/a	n/a	

Covers, Shutters	n/a	TBD	Need for aperture door is TBD by dust contamination analysis

8.3 Marco Polo Camera System MPCS – Close-up Camera CUC

At the moment of writing the accommodation of the close-up imager is not solved. It could be that a location on the robotic (sampling) arm may be feasible but also a location on the S/C body looking downwards maybe a possible solution.

8.3.1 Introduction

This section describes a close-up camera (CUC) compatible with the Marco Polo mission requirements. Scientific issues that can be addressed with this experiment are also identified.

8.3.2 Scientific Goals and Performance Requirements

The main scientific objectives of the CUC can be summarized in the following items (taken from the science requirements document):

SC-010: The regolith size distribution of the actual sampling site shall be measured before and after sampling to sizes as small as 100 μm (goal: 15 μm) in an area about 5 times larger than the area sampled by the sampling device.
SC-040: An additional "local characterisation" shall be performed after the sample collection (i.e. fulfil LR-010 to LR-030 again), for the site where the sample was collected.

The Close-up camera will help to determine physical key properties of the target surface, in order to provide the context to the sample analysis. It will determine the grain size distribution of the regolith, and the composition and aggregation state of loose near-surface materials. The measurements will bear on quantifying weathering processes operating on the asteroid, in terms of local erosion, sedimentation, deposition and precipitation rates close to the landing site. It will also explore the pre- and post-sampling constitution of the surface location where the regolith sample will be taken.

8.3.3 Description

The CUC is a compact imaging device for the 450-900 nm wavelength range designed for microscopic resolution at close object distance. The technical characteristics of CUC depend strongly on the lowest possible (object) distance between CUC and the observation target, which in turn depends on the instrument accommodation. Here, a typical distance of 100cm is assumed. Solar illumination is baseline for the illumination of the surface area to be imaged and no artificial illumination is assumed.

8.3.3.1 Instrument concept

The instrument consists essentially of three key components, i.e. the optics, a focusing unit and a CMOS APS detector with readout electronics (similar to the ones used with the WAC and NAC).

The CUC design is based on a focal ratio of 12.5 and a focal length of 200 mm. The CUC pixel resolution is 50 µm at 100cm surface distance; from that distance the camera will image an surface area of 10 x 10cm at once. Focusing depth is of the order of 1cm such that refocusing may be required to obtain sharp images of the likely uneven surface area at all depths. Focusing is implemented by moving the lens wrt the focal plane. An instrument baffling suppresses straylight.

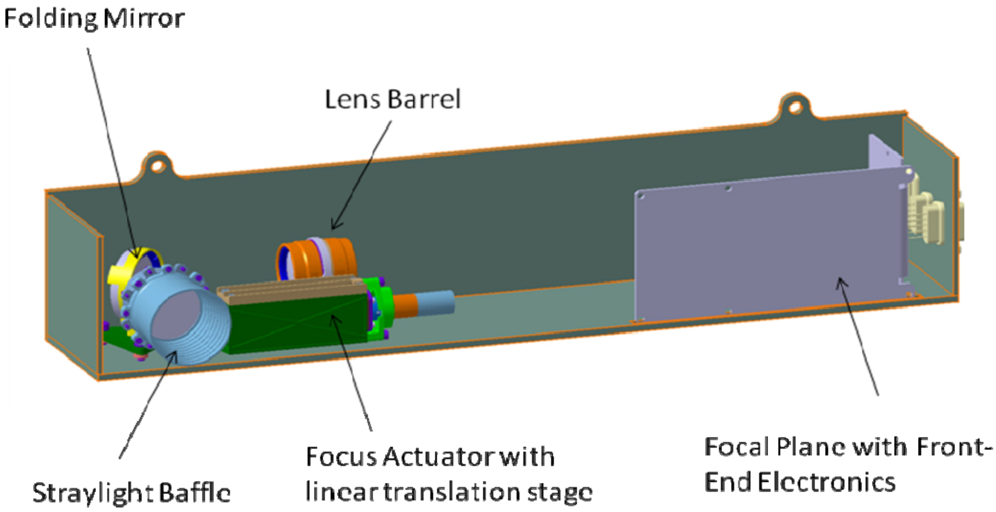

Figure 5 CUC camera – Inside view of the CUC

Figure 6 Example for a CUC – the Rolis camera onboard the Rosetta mission. Note: the rectangular (orange) part above the camera front lens contains the Rolis illumination unit)

The same detector system (active pixel sensor (APS) detector, 2048 x 2048 pixels, 10 x 10 µm pixel size, front-end electronics FEE) as used for the NAC is also used for the CUC. Sensor and FEE are attached to the camera structure.
The instrument is complemented by the common support unit CSU that contains the power control unit PCU and the command and data processing unit CDPU. The CSU serves all three science cameras (WAC, NAC, CUC) onboard MarcoPolo in providing power and handling the command and data processing of the imaging systems and has built-in redundancy.

8.3.3.2 Operation requirements

The CUC will operate before and after each sampling operation. Prior to the acquisition sequence, the camera will be focused. This will be achieved automatically by acquiring several images at different focus distances, and using an algorithm that determines the best focus position based on image contrast. Alternatively, compatibly with the available data volume, the whole set of images taken at different focus positions could be relayed to Earth, so that a 3D reconstruction of the sampling site could be performed. WAC and NAC are assumed to be out of operation while the CUC images are taken at the surface of the asteroid.
Default operation is by timeline; in exceptional cases (commissioning, in-flight problems, special science and focussing applications) commanding and data transmission in interactive mode may be required.

8.3.3.3 Interfaces and physical resource requirements

The CUC camera is fixed mounted pointing into nadir direction. The CSU is mounted separately from the WAC (and NAC, CUC) and is connected with the camera and the spacecraft through Spacewire and power lines. A close arrangement between the WAC, NAC, CUC and CSU is advantageous. Proper temperature range of detector system and opto-mechanics is critical for camera operations and performance quality. Active control may be required.

8.3.3.4 Calibration

The ground calibration activity shall provide the characterisation of the spectral, geometric, radiometric and linearity properties of the camera. These measurements have to be realized on each subsystem (h/w units to be integrated in the CUC).
The CUC in-flight calibration will be based on the observation of selected star fields in order to verify:

- PSF (out of focus)
- Optical axis pointing direction
- Spectral and radiometric calibration

The relative boresight alignment of the CUC may also of interest with respect to other instruments (spectrometer).

8.3.3.5 Cleanliness, planetary protection and pre-launch activities

Normal requirements for cleanliness and pre-launch activities as typical for visible cameras used for space exploration will be applied. Since the instrument is not meant to reach the surface, planetary protection issues are not applicable (except the whole spacecraft crashes or remains in an unintended way on the surface of the NEO).

8.3.3.6 Critical points

The sampling area has to be centered in the field of view of the CUC. Direct solar illumination of the sampling area is required for CUC imaging. Dust contamination by thruster firings during landing and ascent may require the implementation of a dust protection door for the NAC.

8.3.3.7 Heritage

Rolis onboard Rosetta spacecraft and PanCam-HRC, in development for the ExoMars mission

Table 5: Summary table of CUC instrument (Note: CUC operations will require operations of the common support unit CSU for the MarcoPolo camera system consisting of WAC, NAC, and CUC)

Parameter	*Unit*	*Value / Description*	**Remarks**
Reference P/L	n/a	ROLIS, EXOMARS, PANCAM	
Type of optics	n/a	Dioptric	with folding mirror close to entrance

			pupil
Type of camera	n/a	Close-up camera	
OPTICS			
Pupil diameter	mm	12.5	
Focal length	mm	200	
F ratio	n/a	16	
Field of view	°	5.8 x 5.8	
Pixel scale	''/px	10.3	
Spectral range	nm	450 – 900	
Filters	n/a	n/a	
FOCUSING MECHANISM			
Vertical motion	mm	31	
Horizontal motion	mm	n/a	
ILLUMINATIO NUNIT			
Lamp type	n/a	TBD	Current design of CUC relies on Sunlight illumination of the sampling are; usage of illumination unit is under study
Number of lamps	n/a	TBD	
F ratio projection optics	n/a	TBD	
Wavelength resolution	nm	40	
DETECTOR			
Type of detector	n/a	Si PIN-CMOS	Hybrid
Pixel size	µm x µm	10 x 10	
Pixel number		2048x2048	
Exposure time	ms	≤2	
Read out time	µsec/px	0.2	~0.85s read-out time per full frame
Full well capacity	e^-	>120000	
A/D conversion	Bit	14	final raw data: 16 Bit
Operating Temperature	°C	0°C -- + 27°C	
CONFIGURATI ON / LAYOUT			
Units	#	2	Plus shared CSU
Preferred location for sensor	n/a	Focal plane	It's a must (not only preferred)
Preferred	n/a	Compact	

European Space Agency
Agence spatiale européenne

location for electr.		arrangement	
Excitation sources	#	n/a	
Strength of sources	mCi	n/a	
PHYSICAL			
Mass, total (no margins)	g	820	CUC (incl. opto-mechanics, detector, housing, baffling, internal harness) CUC detector FEE
Dimensions (no margins)	mm^3	364X178X68	CUC (incl. opto-mechanics, detector, housing, baffling, internal harness) CUC detector FEE
Sample area	mm^2	50 x 50	Assumed
POWER			
Average (no margins)	W	12.5	CUC focus mechanism CUC detector+FEE +CSU
Peak	W	12.5	
DATA RATE / VOLUME			
Average tm rate	MBit/s	68	Maximum
Data volume per image	MBit	67	
Data volume total (raw data volume, uncompressed)	GBit		
POINTING			
Pointing	µrad	fixed	Centered on sampling area
Pointing accuracy	°	0.1	
THERMAL			
Temperature ranges op. Sensor Head and electronics board	°C	0°C – +27°C	
Temp. ranges op. Deployment-device	°C	n/a	
Temperature ranges Non-op	°C	-60°C -- +40°C	
Temp. ranges Non-op. Deployment-device	°C	n/a	
Temperature stability	°C	1	

CONTAMINATION			
EMC requirements	power supply	TBD	ESA EMC specs to be applied
DC magnetic	n/a	n/a	
Chemical requirements	n/a	n/a	
SUPPORT ITEMS			
Deployment system	n/a	n/a	
Covers, Shutters	n/a	TBD	Need for aperture door is TBD by dust contamination analysis

8.4 Marco Polo Camera System MPCS – Common Support Unit CSU

8.4.1 Introduction

This section describes the common support unit CSU for the visible imaging camera system of the MarcoPolo mission. The CSU is meant to support the operation of the three cameras WAC (wide angle camera), NAC (narrow angle camera), and CUC (close-up camera) of the spacecraft.

8.4.2 Performance Requirements

The main performance requirement of the CSU is the provision of voltages and power as well as providing the command and data processing platform for the three visible cameras WAC, NAC, and CSU of the MarcoPolo imaging system. It shall allow parallel science operation of the WAC and NAC while the spacecraft is in orbit around the asteroid and shall support the operation of the CUC while the spacecraft has landed on the surface.

8.4.3 Description

The CSU is a functional support unit for the MarcoPolo camera system consisting of the WAC, the NAC and the CUC. It is the central operational unit that provides voltages and power for the camera operations, it commands the camera units and processes the data produced by the imaging systems. It is connected to the respective spacecraft interfaces for power, commanding and data transfer.

8.4.3.1 Instrument concept

The CSU consists of two main sub-units, i.e. the power control unit PCU and the command and data processing unit CDPU. Both PCU and CDPU exist in two independent and fully redundant copies (main and redundant PCU and CDPU) within the CSU unit.
Each PCU sub-unit is a distributed system, in which an input power converter provides a regulated bus (28VDC) with regulated low voltage output power (voltage levels of +3.3V and +5V) directly in each unit of the camera system. The PCU includes a housekeeping circuitry to provide status information of the sub-unit (working unit, voltages, temperatures).
The CDPU concept is based on a flexible System-on-Chip (SoC) approach with heritage from DPUs for the VenusExpress camera (VMC) and for the Dawn Framing Camera (FC), both being already in operation in space. The design utilizes a combination of a LEON-3 based processor system together with a set of dedicated, real-time function cores implemented within a high-density reconfigurable Virtex FPGA.
Separate SpaceWire and power lines connect the CSU with the three cameras on one side and with the respective spacecraft interfaces on the other side.

8.4.3.2 Operation requirements

The CSU and its sub-units PCU and CDPU will be operated whenever one of the cameras WAC, NAC, CUC is used. Moreover, it will allow parallel operation of the WAC and NAC and supports – if needed - even operation of all three cameras together. In addition, it can be operated without usage of any of the camera units.

8.4.3.3 Interfaces and physical resource requirements

The CSU is fixed mounted in the spacecraft envelope. It connected with the cameras and the spacecraft through Spacewire and power lines. A close arrangement between the WAC, NAC, CUC and CSU is advantageous.

8.4.3.4 Calibration

N/A.

8.4.3.5 Cleanliness, planetary protection and pre-launch activities

Normal requirements for cleanliness and pre-launch activities as typical for electronic equipment used for space exploration will be applied. Since the unit is not meant to reach the surface, planetary protection issues are not applicable (except the whole spacecraft crashes or remains in an unintended way on the surface of the NEO).

8.4.3.6 Critical points

N/A.

8.4.3.7 Heritage

VMC in VenusExpress, FC in Dawn.

Table 6 Summary table of CSU (Note: The CSU is operated alone and whenever one of the cameras WAC, NAC, CUC is operated.)

Parameter	*Unit*	*Value / Description*	*Remarks*
CONFIGURATION / LAYOUT			
Units	#	1	Unit services are shared between WAC, NAC, CUC
Preferred location for sensor	n/a	n/a	
Preferred location for electr.	n/a	Compact arrangement	CSU electr. is included in CSU except harness
Excitation sources	#	n/a	
Strength of sources	mCi	n/a	
PHYSICAL			
Mass, total (no margins)	g	2900	CSU incl. CDPU and PCU (shared between WAC, NAC, CUC), harness

			between CSU and spacecraft is not included; harness mass: ~150g/m
Dimensions (no margins)	mm^3	250x170x120	CSU incl. CDPU and PCU (shared between WAC, NAC, CUC)
POWER			
Average (no margins)	W	5 8.3 11.2	Mode 0: CDPU+PCU only, no camera operations Mode 1: CDPU+PCU and 1 camera Mode 2: CDPU+PCU and 2 cameras
Peak	W	12.5	Mode 3: CDPU+PCU and 2 cameras and 1 mechanism drive
THERMAL			
Temperature ranges op. Sensor Head and electronics board	°C	-20°C – +40°C	
Temp. ranges op. Deployment-device	°C	n/a	
Temperature ranges Non-op	°C	-60°C -- +80°C	
Temp. ranges Non-op. Deployment-device	°C	n/a	
Temperature stability	°C	1	
CONTAMINATION			
EMC requirements	power supply	TBD	ESA EMC specs to be applied
DC magnetic	n/a	n/a	
Chemical requirements	n/a	n/a	

8.5 MAPIS Visible/Near infrared spectrometer

8.5.1 Introduction

Spectroscopy is an important tool to characterize the composition of planetary bodies.
A visible to near-IR imaging spectrometer is an important instrument to characterize NEOs in order to derive their surface mineralogy, to connect the mineralogical composition with the surface morphology and to map the complete surface of the body. Spectra at different spatial resolution are needed to identify mineralogical provinces on the asteroid surface.

8.5.2 Scientific Goals and Performance Requirements

The following requirement is cited from the Science Requirements Document as reference for the expected scientific performance of this instrument;

GR-020: The complete surface of the NEA shall be imaged in the visible and near-IR wavelength range from 0.4 to 3.3 μm and with a mean spectral resolution $\lambda/\Delta\lambda$ of the order of 200 and a spatial resolution of the order of metres to characterize the mineral properties of the surface (Note: it is acknowledged that depending on the rotation axis of the asteroid there may be areas which cannot be imaged due to illumination constraints).

An imaging spectrometer is required in order to obtain a detailed description of the mineralogical composition of the different geologic units (crater walls and bottoms, ejecta, etc…).
Surface mineralogy and petrology investigation is possible mainly by visible and near-infrared wavelength spectroscopy. Compositional characterizations of asteroids involve analysis of spectra parameters that are diagnostic of the presence and composition of particular mineral species and various materials expected on the target body. Most of the interesting minerals have electronic and vibration absorption features in their NIR reflectance spectra. An identification of the related mineral phases requires a moderate spectral resolution. Organic materials expected on primitive type may be more difficult to evidence and require slightly higher resolution.
Beside that, information about the primary silicates such olivine and pyroxene and their chemistry (abundance of Fe in olivine and of Ca in pyroxene) can be achieved. The relation between ortophyroxene (low Ca) and clinopyroxene (high Ca) can be studied from the analysis of the band position and band strength ratios. Secondary minerals, such as phyllosilicates, have water and OH absorption features at 1.4, 1.9 μm and in the 2.9-3.3 μm range. The presence of the 1.4 and 1.9 μm bands is indicative of undissociated water in the mineral, while the presence of the 1.4 μm band alone suggests OH groups like hydroxyls. The exact position of the bands should be diagnostic of the mineralogy. Similarly, information on the mineralogy of clays and other phyllosilicates can be obtained from the position and relatively intensity of the bands (at 1.4, 1.9, 2.16-2.23 and 2.3 + 2.7 μm) while carbonates have other features in 2.0-3.3 μm range.
In particular asteroid of C taxonomic type (tentatively associated to carbonaceous chondrites) can show in their surface the presence of hydrated silicates, while D types are

expected to including organic materials. In the follow table the position and the width of the detected bands on asteroids are listed:

Table 7 Observed absorption features associated with hydrated minerals on asteroids

Wavelength (μm)	Width (μm)	Transition	Reference
<0.4	>0.1	$Fe^{2+} \rightarrow Fe^{3+}$ intervalence charge	e.g., *Gaffey and McCord* (1979)
0.43	0.02	$6A1 \rightarrow 4A1,4E(G)$ Fe^{3+} spin-forbidden as in jarosite	*Vilas et al.* (1993)
0.60–0.65	0.12	$6A1 \rightarrow 4T2(G)$ Fe^{3+} in Fe alteration minerals	*Vilas et al.* (1994)
0.7	0.3	$Fe^{2+} \rightarrow Fe^{3+}$ in phyllosilicates	*Vilas and Gaffey* (1989)
0.80–0.90	0.08	$6A1 \rightarrow 4T1(G)$ Fe^{3+} in Fe alteration minerals	*Vilas et al.* (1994)
3.0	>0.7	structural hydroxyl (OH) interlayer and adsorbed H_2O	*Lebofsky* (1978, 1980)
3.07	0.2	H_2O ice NH_4-bearing saponite	*Lebofsky et al.* (1981) *King et al.* (1992)

8.5.3 Intrument description

8.5.3.1 Instrument concept

The instrument is a classical slit imaging spectrometer. The spectrometer includes a telescope, a collimator, a low groove density grating, an objective and the focal plane. A shutter is placed in front of the entrance slit to subtract background images. Due to the low groove density of the grating, a sorting order filter is placed in front of the detector. Its variable band pass along the spectrum not only rejects unwanted orders, but also reduces background seen by each pixel.

On a two-dimension detector, this kind of imaging spectrometers records a 1D image and a full spectrum for each point of the 1D image. Either the relative displacement of the S/C with respect to the asteroid or a scanning system are needed to recover the second spatial dimension. In order to simplify complex S/C balancing modes, a scanning device is proposed.

An internal spectral calibration system using Fabry-Perot, allows to check the spectral registration before each sessions. The scanning system is used to point the calibration device.

It is assumed that a DCDC convertor is provided by the instrument main electronics.
The proximity electronic is based on an ASIC and a FPGA minimizing its mass and volume
The instrument and the detector shall be cooled by means of radiator. The typical detector temperature will be 150K
The instrument depth of focus is sufficient to allow observation during this phase without degradation of the performances. Therefore the instrument can observe at all operation phases (FAR, TER, GLO, LOC).
Note: Two slit spectrometers are under study within the consortium. MAPIS (Marco Polo Imaging Spectrometer) and SETA (Spectral Experiment for Target Asteroid)

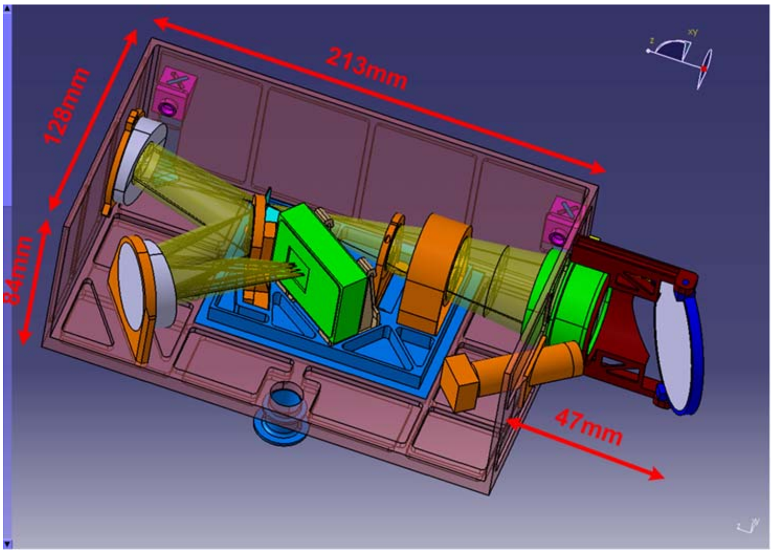

Figure 7 One of the proposed imaging spectrometer

In Figure 8 a sketchmap shows the key components of the proposed design of the instrument.

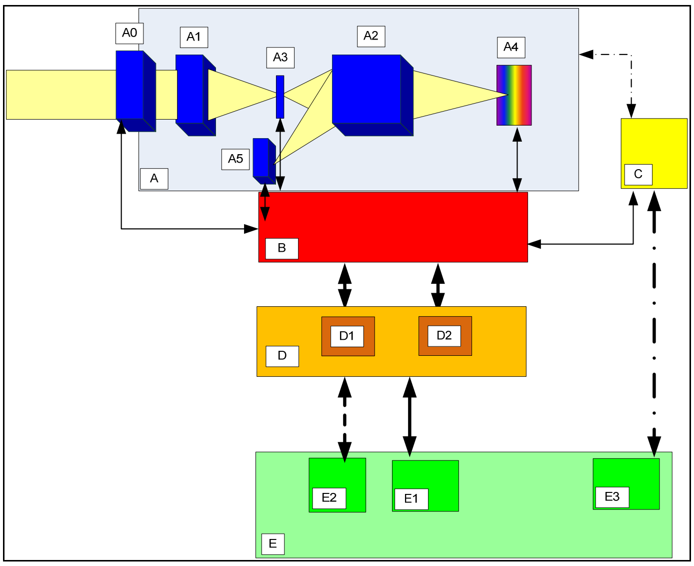

Figure 8 Sketchmap of the Vis NIR spectrometer

A) Optical head
A0) Scanner sub-system - A1) Collecting sub-system – A2) Dispersing and imaging sub-system – A3) spatial filtering and shutter sub-system – A4) Spectral image and detector – A5) radiometric calibration sub-system
B) Proximity electronics
C) Cooling system
D) Main electronics
D1) DCDC converter – D2) DPU board
E) Spacecraft resources
E1) 28V – E2) TM/TC – E3) Thermal well

8.5.3.2 Orbit, operations and pointing requirements

=> THIS chapter needs a revision for 1996 FG3 <=

The instrument will make the spectral mapping of the complete surface of the asteroid. It **only** operates when observing **daylight side**.
The baseline target is **1999JU3**

At S/C level, 5 mission phases are considered:

- Formation flying (FAR)
- Terminator orbit (TER)
- Global characterisation (GLO)
- Local characterisation (LOC)
- Landing

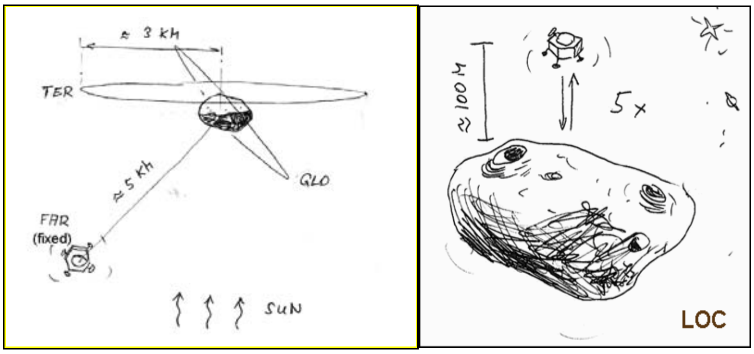

Figure 9 Sketch of the FAR, TER, GLO and LOC mission phases

In the following, the asteroid is considered as a sphere with a diameter of 0.78km
For each phase the orbit is considered circular.

Table 8 Operation parameters

Phase mode	S/C distance to asteroid	Pixel size on object	Data volume to cover object(1)
FAR	5km	1.25m	5Gbit
TER	3km	0.75m	14Gbit
GLO	2km	0.5m	33Git
LOC	100m	0.025m	10Gbit(2)

Landing	N/A	N/A	N/A

(1) Apart from LOC, coverage of the overall surface. No compression, no redundancy, no calibration

(2) Assuming a total time for this phase of 1 hour. No compression, no calibration

Remarks:

TER phase:

The instrument can operate in this phase only if the phase angle is high enough at least to reach the illuminate side but also to prevent straylight (imaging spectrometers does not work well for low phase angles).

LOC phase:

The instrument depth of focus is sufficient to allow observation during this phase without degradation of the performances.

Table 9 Operating modes versus power consumption of the VisNIR spectrometer

Operating modes			
		Calibration	*operations*
	Goal	Spectral using an internal lamp	Close or far mapping
	Duration	30 sec	8 weeks
	Power average	20W (1)	20W (1)
	Additional peak power	3W (2)	1W (3)
	Operational constraints	N/A	N/A
	Number of occurrence of the operation	every 500 spectral images	

(1) Average power: 16W + 25% efficiency of DC/DC converter = 20W
3W for 3.3V devices
7W for cooler
6W for ME (including DC/DC convertor)

(2) Peak power: 3W
2W for calibration
1W for shutter (3)

8.5.3.3 Interfaces and physical resource requirements

The instrument alignment with the NAC/WAC shall be known within an accuracy of 0.12 mrad corresponding to half a pixel field of view.
Radiators should stay in the shadow during operations

8.5.3.4 Calibration

The in-flight spectral calibration shall be performed by pointing external sources such as stars or planets. This pointing will also be used to cross check instruments co-alignments. The conception of the instrument shall be done to minimize the number of occurrences of this operation.

The in-flight radiometric calibration shall be done using internal sources lighting the pupil. This calibration will be used to monitor the variation of the instrument spectral response. This operation shall be done at the beginning and the end of each session.
If possible, ideally, a radiometric calibration could be done by pointing a spectrally flat external source such as the moon when it is close enough to fill the instrument FOV.
Calibration data volume: 1Mbit per session without compression (includes one full, uncompressed image of the Fabry-Perot spectral lines and one full, uncompressed background image obtained by closing the shutter).

8.5.3.5 Cleanliness, planetary protection and pre-launch activities

No specific requirements

8.5.3.6 Critical points

At this point of the study, the main critical point is the mass of the instrument. We estimate a margin of 20% of the nominal value.

8.5.3.7 Heritage and TRL assessment

The heritage comes from:
Development of the overall optical head and proximity electronics of IR imaging spectrometers for MarsExpress, Rosetta and VenusExpress.
Strong contribution in mission payloads for BepiColombo, Hayabusa, ExoMars, SMART-1 / Chandrayaan-1

The assessment of the technology readiness level provides the following result;

Table 10 MAPIS TRL assessment

		TRL	Rational
Optical Head			
	Telescope	5	All materials qualified on previous exploration missions
	Slit	5	Qualified on previous exploration missions
	Shutter	5	Qualified on previous exploration missions
	Collimator	5	Qualified on previous exploration missions
	Grating	5	Qualified on previous exploration missions
	Objective	5	Qualified on previous exploration missions
	Detector	5	Use of a wavelength and size adapted 6604b detector that reaches TRL5 by the end of 2009 and will be at TRL 6/7 in 2011. The precursor detector 6604a is already flight proven (TRL 9).
	Filter order sorting	4-5	Studied on previous R&D program.
	Scanner		
	Fabry-Perot	5	Qualified on previous exploration missions
	FP lamp	5	Qualified on previous exploration missions

	FP lens	5	All materials qualified on previous exploration missions
	Optical bench	5	Qualified on previous exploration missions
	Housing	5	Qualified on previous exploration missions
	Feet	5	Qualified on previous exploration missions
	Radiator	5	Qualified on previous exploration missions
	MLI	5	Qualified on previous exploration missions
	Int cabling	5	Qualified on previous exploration missions
Electronics			
	Elec boxes	5	Qualified on previous exploration missions
	Proxim. Electronic	5	Qualified on previous exploration missions
	Analog circuitry	5	Radiation hard operational amplifiers
	Control	9	ACTEL RTSX32SU controls the camera system
	Main electronic	5	Qualified on previous exploration missions
Cables			
	Cryo	5	Qualified on previous exploration missions
	SpaceWire PE/DPU	9	Aeroflex SpaceWire circuits are available
	Space Wire SPU/SC	5	Qualified on previous exploration missions
EGSE		N/A	

8.5.3.8 Summary table

Table 11 Description summary of the VisNIR spectrometer

Parameter	Units	Value/Description	Remarks
Heritage P/L	n/a	Rosetta / BepiColombo/ Hayabusa / MarsExpress / SMART-1 / Chandrayaan-1	
Type of instrument	n/a	imaging IR spectrometer	
Type of optics	n/a	Mirrors and grating	
Type of detectors	n/a	MCT	Mercury-Cadmium-Telluride
OPTICS			
Spectral Range	µm	0.4-3.3 µm	
FOV	mrad	32	
Pixel IFOV	mrad	0.25	
Aperture	mm	40	
Focal length	mm	120	
Focal number	#	3	
Spectral Channels	#	1	
spectral resolution	$\lambda/\Delta\lambda$	>100	λ>1µm
Signal to noise ratio	n/a	>100	
Detector			
Type of detector		MCT	
Pixel lines in array	#	128	
Pixels per array line	#	311	
Pixel size	µm	30	
Exposure time	msec	100	
Repeat time	msec	500	
Operating temperature	°C	-123	
A/D conversion	bit/pix	14	
Full well capacity	ke-	1000	
Readout time	msec	10	
SWATH and RESOLUTION			
Swath width @ 5km	km	0.16	
Swath length @ 5km	M	1.25	
Spectral sampling	nm	10	@ FWHM
Angular resolution	mrad	0.25	
Spatial (pixel) resolution @ 5km	M	1.25	
PHYSICAL			
Mass, total	G	3600	4.3kg with 20% margin.

Dimension	mm	260x128x84 150x180x65	Optical head (includes scanning syst) Main electronic
Footprint		312x128 150x65	2 boxes (optical head and main electronic)
POWER			
Total average power	W	18	Without cooler
Power (peak)	W	25	Includes cooler
Cooler	W	7	
Data			
Data rate		2.8Mbit/s	
Cube volume		0.5 Mbit	
Data volume (whole body)			
Compression factor		10 max – 7 nominal - 3 lossless	

8.6 Mid IR spectrometer

8.6.1 Introduction

Mid-infrared spectroscopy provides information on the surface mineralogy (silicates and organics), the surface temperature, thermal inertia and presence and properties of regolith. The compositional information complements the data obtained form UV-Vis-NIR spectrosocopy and provides global context for the returned samples. Spectroscopic maps are used to determine the surface temperature distribution which, with the use of thermal models, can constrain the surface thermal inertia and dominant regolith particle size. These properties will be used to inform the sample site selection. In addition, they provide valuable information for determination of sizes and albedos from optical and IR observations of unresolved NEOs using the radiometric method and study of the Yarkovsky effect.

8.6.2 Scientific Goals and Performance Requirements

The following requirements are cited from the Science Requirements Document as reference for the expected scientific performance of this instrument;

GR-050: The surface temperature of the complete NEA shall be derived to an accuracy of at least 5 K (goal 1 K) above 200 K (tbd). The spatial resolution shall be of the order of 10 m at a number of rotational phases from which the thermal inertia can be determined to a precision of better than 10 %
GR-060: The complete surface of the NEA shall be imaged in the mid-IR with a spatial resolution of the order of 10m or better and with a spectral resolution of λ/Δλ of the order of at least 200 to determine the wavelength dependent emissivity, and hence identify mineral features in the range 8 – 16μm (goal 5 – 25μm).
LR-020: A representative area within the expected landing area ellipse (goal: entire ellipse) shall be imaged in the visible and near-IR wavelength range to characterise the mineral properties of the surface with a mean spectral resolution of λ/Δλ of the order of 200 and a spatial resolution of the order of decimetres to characterize the mineral properties of the surface.

8.6.2.1 Objectives

The objectives of a mid-IR spectrometer are to

- Derive the surface temperature to an accuracy of at least 5 K (goal 1 K) at a spatial resolution of the order of 10 m at a number (*tbc*) of rotational phases from which the thermal inertia can be determined to a precision of better than 10 % .
- Map the complete surface of the NEO with a spatial resolution of the order of 10 m or better to identify silicate spectral features in the 9 – 11 μm (and optionally in the 5-8 μm and 18-22 μm bands) with a spectral resolution of at least λ/Δλ in the order of 200.

8.6.2.2 Thermophysical properties

Typical surface temperatures for an NEO at a heliocentric distance of 1 AU range from as low as 100 K in unilluminated areas to almost 400 K near the subsolar point for a slow rotating low thermal inertia object. Diurnal cycles in the asteroid surface temperature are strongly dependent on the thermal and physical properties of the top several centimetres of the surface. Many factors have an effect on temperature, including albedo, but thermal inertia is the key parameter. Thermal inertia is defined as a combination of thermal conductivity K, density ρ, and specific heat capacity CP: $\Gamma = \sqrt{K\rho C_P}$, and represents the ability of the subsurface to store and conduct heat energy away from the surface during the day and to return that heat energy to the surface through the night. Deriving and understanding the thermal inertia of a surface can help to identify the small-scale characteristics of that surface. Fine grained and loosely packed material typically exhibits a low value of thermal inertia, while higher values are common for rocks and exposed bedrock.

The surface and subsurface temperature of a surface element of an NEO can be calculated using a thermophysical model, where the thermal diffusion equation is solved for subsurface temperatures by a forward-time finite-difference method, with the appropriate boundary conditions. Synthetic spectra are then derived and fitted to observed IR spectra to constrain the thermophysical properties. Recently, sophisticated thermophysical models have been applied to NEOs, modelling their known shapes and pole orientations, in order to determine their surface thermal inertia Γ. Mueller et al. (2007) found Γ = 150 J m-2 K-1 s-1/2 (all subsequent values are in these units) for (433) Eros and Γ = 350 for (25143) Itokawa. Harris et al. (2005) measured Γ = 180 for (1580) Betulia and Mueller et al. (2007) determined Γ = 150 for (33342) 1998 WT24. Thus, the average NEO surface inertia appears to be considerably greater than that of (large) main belt asteroids (MBAs): Müller and Lagerros (1998) obtained Γ = 5-25 for five MBAs using the Infrared Space Observatory. Delbó et al. (2007) have found the average thermal inertia to be 200 ± 40. All these values lie between the expected extremes of 40 (fine particulate dominated surface such as the lunar regolith) and 2200 (solid rock, e.g. granite).

These data have been obtained from disk integrated models observed at one geometry (solar phase angle) and are therefore an average of the overall surface visible at that time. Spatially resolved data obtained at a range of rotational phases and local phase angles will allow the influence of local topography, (shadowing and beaming) and regolith properties (composition, size distribution) to be studied and provide more powerful constraints on the surface conditions.

Kieffer et al. (1977) discuss what may be inferred about Martian surfaces from measurements of Γ, which can also be applied to asteroid surfaces. The principal thermophysical property determining inertia is the conductivity (k) which is closely related to particle size [e.g., Kieffer et al. (1973), Palluconi and Kieffer (1981), Jakosky (1986)]. Assuming a uniform particle size and a smooth, homogeneous surface, the thermal conductivity of the bulk material is strongly affected by the particle diameter [e.g., Wechsler and Glaser (1965), Presley and Christensen (1997)], varying by several orders of magnitude, while density and heat capacity change little. Therefore, thermal inertia will also vary significantly with particle size. Lower thermal inertias (about Γ ≤ 170) may indicate a surface covered with fine particles with diameters less than about 0.1 mm. Γ ≥

170 may be due to: particle distributions with mean particle diameter greater than 0.1 mm; distributions of small particles, larger blocks and exposed bare rock, or surfaces consisting of bonded fine particles.
In addition to the derivation of near-surface properties, the thermal inertia is a key parameter in determination of the Yarkovsky effect, caused by anisotropic emission of thermal photons, which is the dominant long term perturbing force for km sized bodies and provides the key for dynamical transfer from the main belt.
It can be seen that it is difficult to interpret values of thermal inertia because a great variety of surface types can result in the same area average thermal inertia. The spatial and rotational phase resolution of in-situ data, and the further constraints on surface properties from other instruments (particularly if a separate lander is included) will allow major advances to be made.

8.6.2.3 Composition from Mid-IR spectra

Emission spectra in the thermal infrared are well suited to addressing silicate mineralogies. This spectral region contains the Si-O stretch and bend fundamental molecular vibration bands (typically in the ranges 9-12 and 14-25 µm, respectively). Interplay between surface and volume scattering around these bands creates complex patterns of emissivity highs and lows which are very sensitive to, and therefore diagnostic of, mineralogy as well as grain size and texture. The three main types of feature observed in mid-IR spectra are:
Christiansen features are due to rapid changes in the refractive index are responsible for an anomalous dispersion that makes the particulate sample transparent. This phenomenon produces the appearance of the Christiansen features at shorter wavelength with respect to the reststrahlen features. The Christiansen feature, which is directly related to the mineralogy and the grain size, appears in the spectra between 8 and 9.4 µm.
Reststrahlen features are due to the vibrational modes of molecular complexes. The absorption coefficient at resonance wavelengths is very strong producing the most intense bands in the infrared spectrum by surface scattering. They are strongly depended on grain sizes; for smaller grain sizes, the main reststrahlen features decrease their spectral contrast. These features are visible between 9 and 12 µm and at wavelength larger than 20 µm.
Transparency features. In the spectral region where the absorption coefficient decreases, grains become more transparent. Usually, this occurs at 11-13 µm between main restrahlen bands and at longer wavelengths (> 30 µm) where the absorption coefficient decreases. If the grain size is small, volume scattering occurs and transparency features are observable due to a loss of photons crossing many grains.
Many of the major rock-forming elements and their complexes have fundamental vibration frequencies corresponding to mid- and thermal-IR wavelengths, 5–50 µm. Nearly all silicates, carbonates, sulfates, phosphates, oxides, and hydroxides show mid-IR and thermal IR spectral signatures [e.g., Lyon (1962); Hunt and Salisbury (1974), (1975), (1976); Farmer (1974)] Bands in the 4–7-µm region are mostly over-tones and combination tones of the stretching and bending of SiO and AlO fundamentals with some lattice modes present in minerals. Also, carbonates have strong absorptions from CO_3 internal vibrations in the 6–8-µm region; these bands are easily distinguished from silicate absorptions [Adler and Kerr (1963); Hunt and Salisbury (1975)]. Hydroxide-bearing minerals (clays) also have characteristic mid-IR spectra [Van der Marel and Beutelspacher (1976)], with spectral

features from the fundamental bending modes of OH attached to various metal ions, such as an H-O-Al bending mode near 11 μm in kaolinite [Hunt (1980)]. Phosphates and sulfates also have diagnostic absorption bands associated with their anion complexes (PO 3–4 and SO 4–4), as do oxides, nitrites, and nitrates. Sulfides and halogenide salts are also readily distinguished [Hunt and Salisbury (1975)].

The interpretation of the continuum of reflectance or thermal emissivity of an asteroid surface is difficult and not unique, since asteroid surfaces are composed of mixtures of minerals whose spectral properties are non-linearly combined. Asteroid spectra are affected not only by the chemical composition of the surfaces, but also by several physical parameters, such as particle size, porosity, packing, and thermal gradients [Logan et al. (1973); Salisbury and Estes (1985); Salisbury and Walter (1989), Arnold (1991); Ruff et al. (1997); Lane and Christensen (1998); Lane (1999); Harloff and Arnold (2001)]. These effects only become significant as the particle size becomes small (<~100 μm) and are most important as the size approaches the wavelength being observed (e.g. Salisbury and Walter (1989)).

Because of their spectral similarity in the visible and near-infrared regions, C-type asteroids have always been associated with CI and CM meteorites especially due to their matching weak absorption features in the shortest wavelength regions. Mid-infrared spectroscopic (2-25 microns) analysis will give further stronger constraints on this subject. Cohen *et al.* (1998) and Witteborn *et al.* (2000) interpreted emissivity features in spectra of (1) Ceres obtained on board the Kuiper Airborne Observatory (KAO) as indicative of fine-grained olivine. Barucci *et al.* (2002) and Dotto *et al.* (2004) report Infrared Space Observatory (ISO) spectra of two low albedo asteroids: 10 Hygiea (C-type) and 308 Polyxo (T-type). The spectra of both objects exhibit an emission plateau near 10 μm. The Hygiea spectrum rises somewhat slowly longward of this to a peak near 20 μm, whereas the Polyxo spectrum has a narrower transparency minimum centered near 12.5 μm, similar to CO3 meteorite and crystalline olivine spectra. These authors also note similarities to carbonaceous meteorites and that small grain sizes are required to reproduce the 10-μm plateau.

Theoretical approaches, developed by Hapke (1981, 1993) and Shkuratov *et al.* (1999), can be used to model the thermal emission of the asteroid particulate surface using the optical constants of the suitable materials.

8.6.2.4 Requirements of Mid-IR spectrometer

We require an instrument capable of measuring the surface temperature to a precision of a few K from which the thermal inertia and other surface properties can be constrained.

The instrument should operate between 5 and 25 microns to sample the wide range of mineralogical features in the mid-IR and ensure good sampling of the thermal emission for temperatures from 100 to 400 K.

A spectral resolution of at least 100 is required to provide good sampling of emission features and continuum.

A spatial resolution of order 10m is required to sample approximately isothermal regions, separate different factors influencing the thermal inertia and derive local properties required for potential landing site definition.

Observations of each surface element at a range of rotational phases provide much greater constraints on the properties by reducing thermal model redundancies.

8.6.3 Description

8.6.3.1 Instrument concept

The instrument is an imaging Fourier transform mapping spectrometer utilising a beam-shearing interferometer to generate a set of spatially resolved interferograms that are imaged onto a detector array. This allows spectral image cubes of the target body to be measured. The instrument covers the key spectral range of 400 to 2000 cm^{-1} with a maximum programmable resolution of $10cm^{-1}$. The extended spectral range is vital, as it includes important diagnostic mineral absorption bands as well as the thermal continuum due to the full diurnal temperature range of the object.

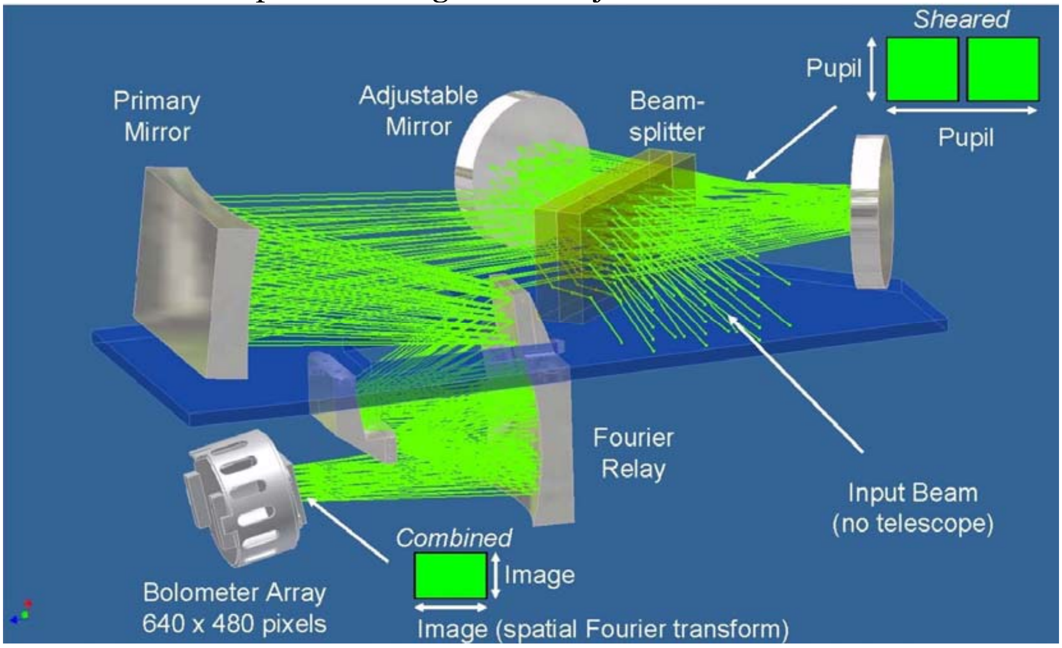

Figure 10. The ATMS breadboard optical layout. The dimensions are 160 x 220 x 370 mm^3 – but note the instrument is not box shaped.

The proposed instrument (*Figure 10*) is the latest in a series of interferometers designed by F. Reininger of SpiLab, first breadboarded at JPL, and with later versions developed at SpiLab incorporating actively cooled optics and detectors, and then a flight like version assembled and tested in Oxford with passively cooled optics and detectors. The instrument uses a mid-infrared beam splitter and all reflective optics to image the interferogram on to a 640x480 micro-bolometer array, rather than using a traditional moving mirror arrangement. The mirrors are fabricated from aluminium alloy and are incorporated into their mounts. This leads to a highly reliable, compact, low mass and low power instrument with no moving parts except a rotary scan/calibration mirror assembly. The scan mirror is essential to allow measurements of space and of a low power miniature black body target to maintain radiometric calibration during operation. The rotation axis of this scanning mirror is oriented so that a single mechanism can perform this calibration as well as scanning the field of view across the asteroid.

8.6.3.2 Orbit operations and pointing requirements

=> THIS chapter needs a revision for 1996 FG3 <=

The image cube generated by the instrument is illustrated in figure 2. The asteroid is mapped by scanning the 480 cross track pixels across the surface. To maximise signal to noise, the measurements along the 640 pixel axis do not correspond to the same point on the target. Instead these must be scanned to assemble the interferogram of each single point.

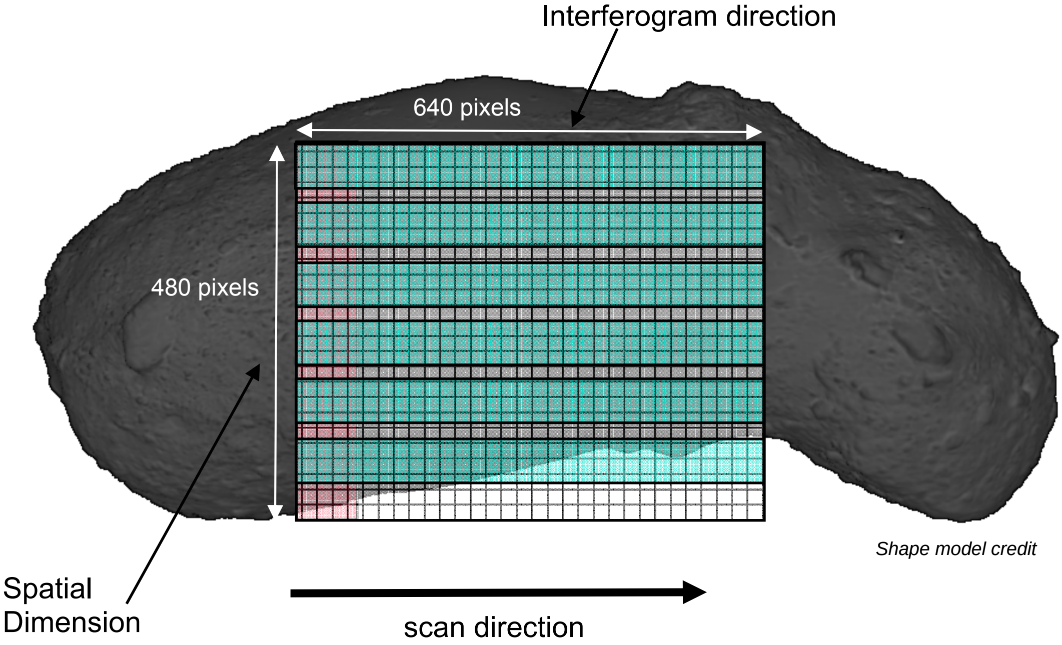

Figure 11. Scanning for the ATMS instrument.

The instrument is ideally suited to a "pushbroom" measurement approach in which the motion of the spacecraft around the target body provides the scanning to build up the interferograms. For most of the potential Marco Polo targets, however, the drift of the field of view due to the target body is comparable with that caused by the spacecraft motion. For the approach to be acceptable the orbit direction would have to be aligned with the rotation so that the cross track motion is less than about 10% of the along track. The "pushbroom" approach remains a potential operating mode for some targets under consideration and could potentially reduce power consumption.

Table 12 Geometrical and motional constraints for 1999 JU3

		1999 JU3	**1999 JU3**	1999 JU3	1999 JU3
asteriod diameter	m	720	**1080**	720	1080
asteroid mass	Kg	2.15E+11	**9.89E+11**	2.15E+11	9.89E+11
orbit radius	m	2500	**2500**	5000	5000
rotation rate	h	7.7	**7.7**	7.7	7.7
asteroid density	Kg/m3	1100	**1499**	1100	1499
asteroid circumference	m	2262	**3393**	2262	3393
orbit period	h	57.6	**26.9**	162.9	76.0
orbit speed	m/s	0.0757	**0.1624**	0.0536	0.1149
ground speed from orbit	m/s	0.0109	**0.0351**	0.0039	0.0124
ground speed from rotation	m/s	0.0816	**0.1224**	0.0816	0.1224
ifov	m	0.54	**0.49**	1.16	1.12

Table 12 lists some operational constraints for the nominal cases adopted for target 1999 JU3. The column in bold text is used as a case for the illustrative calculations below. For this nominal case, the rotation of the asteroid is the dominant cause of drift of the field of view. It is unlikely that our advance knowledge of the rotation would allow us to orient the orbit and spacecraft to utilise this drift, also the drift rate is slow so that it would take several thousand seconds to build up a complete interferogram cube. Instead the instrument uses a micro-stepping rotary mechanism to step along the scan direction. This nominal operating mode is illustrated in Figure 12.

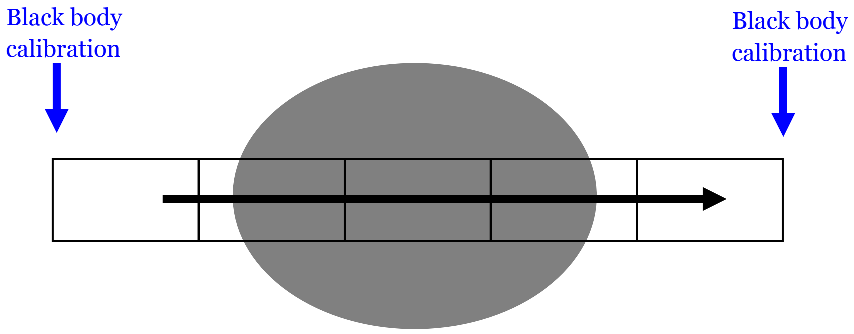

Figure 12 ATMS nominal scanning mode

The sample time of the detector array is 50msec and a complete scan across the asteroid will take typically ~200 seconds including settling time and complete frames viewing cold space to provide a zero reference. Black body views at the start and end of the scans mean that each observation sequence includes all information needed for calibration.
Data will be averaged within the instrument's internal FPGA differently for the two axes of the array. Averaging across the track (the spatial dimension) will be determined by the desired resolution, typically averaging 10 pixels for 1999 JU3 to reach 5m. Along the 640 pixel dimensions 3 points will normally be averaged since only 210 samples are needed to achieve the desired resolution. The FPGA will include the capability of excluding any bad pixels. In addition, each sample will be averaged in time to match the scan rate and spatial resolution. The data volume returned to Earth will thus be determined by the programmed resolution, not by the potential data rate produced by the array.

Ideally, to map the asteroid efficiently, the scan direction would be orthogonal to the orbit drift caused by rotation and spacecraft motion. The scan would therefore be repeated every 30 minutes (0.49*480/0.122 seconds) to map the whole asteroid using 10 strips with a small overlap.
The expected data rate for a single complete asteroid map in this nominal case is therefore: 10 strips x 48 cross track pixels x 233 along track pixels x 210 interferogram points = 23.5×10^6 samples or 44.8 Mbytes.
The interferograms produced will be very similar to those from the Cassini/CIRS instrument for which we have routinely demonstrated compression ratios of 2.5 so 18Mbytes per map is a good estimate for 1999 JU3. Ten maps will be sufficient to provide the required phase angle coverage and to allow for repeated maps to provide better polar resolution. High spatial resolution maps of selected areas of the surface are also highly desirable.

8.6.3.3 Interfaces and physical resource requirements

Four Fixation points. Power connection 0-28V data and commands serial interface
Instrument alignment, if practical, so that scan mirror rotates field of view across the direction of peak surface motion caused by rotation or spacecraft motion.

8.6.3.4 Calibration

Since accurate surface temperature measurement (±0.2K) is a primary requirement for robust determination of surface properties due to variations in their thermal signature, a scan pattern that includes regular views of the internal calibration target and space is essential.

8.6.3.5 Cleanliness, planetary protection and pre-launch activities

Bio-cleanliness at COSPAR level 4B has been established in Oxford's assembly facility for Exomars. It is assumed that since the ATMS will make no contact with the asteroid surface the level required will be significantly lower than this.

8.6.3.6 Critical points

Modulation efficiency of the revised interferometer to be demonstrated.
Detector array noise performance to be demonstrated.
Flight compatible scan mirror mechanism to be demonstrated.

8.6.3.7 Heritage

Several breadboard instruments using the spatially modulated concept have been assembled and tested, including demonstration systems with actively cooled optics and detectors (e.g. Reininger 2001) and a compact flight-like breadboard with passively cooled optics and detectors (Mortimer 2008).

8.6.3.8 References

Adler, H. H.; Kerr, P. F. (1963) Infrared spectra, symmetry and structure relations of some carbonate minerale. *Am. Mineral.*, 48, 839-853.

Arnold, G., (1991). Measurements of the spectral emittance of particulate minerals and some remote sensing implications, *Vibrational Spectroscopy*, 2, 245-249.

Barucci, M.A., Dotto, E., Brucato, J.R., Muller, T.G., Morris, P., Doressoundiram, A., Fulchignoni, M., De Sanctis, M.C., Owen, T., Crovisier, J., Le Bras, A., Colangeli, L. and Mennella, V. (2002). 10 Hygiea: ISO infrared observations. *Icarus* 156, 202-210.

Cohen, M., Witteborn, F.C., Roush, T., Bregman, J. and Wooden, D. (1998). Spectral irradiance calibration in the infrared. VIII. 5-14 micron spectroscopy of the asteroids Ceres, Vesta, and Pallas. *Astron. J.,* 115, 1671-1679.

Delbó, M. (2004). The nature of near-Earth asteroids from the study of their thermal infrared emission. PhD thesis, Freie Universität, Berlin.

Delbó, M., dell'Oro, A., Harris, A.W., Mottola, S. and Mueller, M. (2007). Thermal inertia of near-Earth asteroids and implications for the magnitude of the Yarkovsky effect. *Icarus* 190. 236-249.

Dotto, E., Barucci, M.A., Brucato, J.R., Muller, T.G. and Carvano, J. (2004). 308 Polyxo: ISO-SWS spectrum up to 26 micron. *Astron. Astrophys.* 427, 1081-U1130.

Farmer, V.C. (1974). Infrared spectra of Minerals, *Mineral Society*, London,

Hapke, B. (1981). Bidirectional reflectance spectroscopy. I – Theory. *J. Geophys. Res.*, 86, 3039-3054.

Hapke (1993) *Theory of Reflectance and Emittance Spectroscopy*, edited byR. E. Arvidson and M. J. Rycroft, Cambridge Univ. Press, New York

Harloff, J. and Arnold, G. (2001). Near-infrared reflectance spectroscopy of bulk analog materials for planetary crust. *Planet. Space Sci.* 49, 191-211.

Harris, A.W., Mueller, M., Delbò, M. and Bus, S.J. (2005). The surface properties of small asteroids: Peculiar Betulia - A case study. *Icarus* 179, 95-108.

Hunt, G. R., (1980). Electromsgnetic radiation: The communication link in remote sensing, in Remote Sensing in Geology, B. S. Siegal and A. R. Gillespie eds, Wiley, New York, pp. 4-45.

Hunt, G. R., and Salisbury, J. W. (1974). Mid-Infrared spectral behavior of ignous rocks, *Environ. Res. Paper*, 496-AFCRL-TR-74-0625, p. 142.

Hunt, G. R., and Salisbury, J. W., (1975). Mid-Infrared spectral behavior of sedimentary rocks, *Environ. Res. Paper*, 520-AFCRL-TR-750356, p. 49.

Hunt, G. R., and Salisbury, J. W., (1976). Mid-Infrared spectral behavior of metamorphic rocks, *Environ. Res. Paper*, 543-AFCRL-TR-76-0003, p. 67

Jakosky, B.M. (1986). On the Thermal Properties of Martian Fines. *Icarus* 66, 117-124.

Kieffer, H.H., Chase, S.C., Miner, E., Munch, G. and Neugebau.G (1973). Preliminary Report on Infrared Radiometric Measurements from Mariner-9 Spacecraft. *J. Geophys. Res.* 78, 4291-4312.

Kieffer, H.H., Martin, T.Z., Peterfreund, A.R., Jakosky, B.M., Miner, E.D. and Palluconi, F.D. (1977). Thermal and Albedo Mapping of Mars During the Viking Primary Mission. *J. Geophys. Res.* 82, 4249-4291.

Lane, M. D., (1999). Mid infrared optical constants of calcite and their relationship to particle size effects in thermal emission spectra of granular calcite, *J. Geophys. Res.*, 104, 14099-14108 .

Lane, M. D., and Christensen, P. R., (1998). Thermal Infrared Emission Spectroscopy of Salt Minerals Predicted for Mars, *Icarus*, 135, 528-536.

Logan, L. M., et al., (1973). Compositional implication of Christiansen frequency maximum for infrared remote sensing applications, *J. Geophys. Res.*, 78, 4983-5003.

Lyon, R. J. P., (1962). Evalutation of infrared spectrophotometry for compositional analysis of lunar and planetary soils, Stanford Res. Inst. Final Rep. Contract, NASA, 49-04

Mortimer et al. (2007). Development of a miniaturised remote sensing interferometer American Astronomical Society, DPS meeting #39, #34.09

Mortimer et al 2008. D. Phil Thesis University of Oxford 2008

Mueller, M., Delbó, M., Kaasalainen, M., Di Martino, M., Bus, S. and Harris, A.W. Indications for regolith on Itokowa from thermal-infrared observations. PASP Conference Series. (2007) in press.

Müller, T.G. and Lagerros, J.S.V. (1998). Asteroids as far-infrared photometric standards for ISOPHOT. *Astron. Astrophys.* 338, 340-352.

Palluconi, F.D. and Kieffer, H.H. (1981). Thermal Inertia Mapping of Mars from 60-Degrees-S to 60-Degrees-N. Icarus 45, 415-426.
Presley, M.A. and Christensen, P.R. (1997). Thermal conductivity measurements of particulate materials .2. Results. *J. Geophys. Res.-Planets* 102, 6551-6566.
Reininger (2001) A Spatially Modulated Interferometer for mapping Maritain water vapour Sources. D.Phil Thesis Univ. Oxford 2001.
Reininger F. M. Infrared Physics and Technology 42 (2001) 345-362.
Ruff, S. W., Christensen, P. R., Barbera, P. W., Anderson, D. L. (1997). Quantitative thermal emission spectroscopy of minerals: A laboratory technique for measurement and calibration, *J. Geophys. Res.*, 102, 14899-14913.
Salisbury, J. W., and Estes, J. W. (1985). The effect of particle size and porosity on the spectral contrast in the midinfrared, *Icarus*, 71, 586-588.
Salisbury, J. W., Walter, L. S., and D'Aria, D. (1988). Mid-infrared (2.5 to 13.5 μm) spectra of igneous rock, *U. S. Geol. Surv. Open File Report*, Reston, Virginia
Salisbury, J. W., and Walter, L. S., (1989). Thermal infrared (2.5-14.5 μm) spectroscopic remote sensing of ignieous rock types on particulate planetary surface, *J. Geophys. Res.*, 94, 9192-9202.
Shkuratov, Y., Starukhina, L., Hoffmann, H., Arnold, G. (1999). A Model of Spectral Albedo of Particulate Surfaces: Implications for Optical Properties of the Moon, *Icarus*, 137, 235-246.
Van der Marel H. W. and Beeutelspacher H., (1976). Atlas of Infrared Spectroscopy of Clay Mineral and their Admixtures, Elsevier, Amsterdam
Wechsler, A.E. and Glaser, P.E. (1965). Pressure Effects on Postulated Lunar Materials. *Icarus* 4, 335-&.
Witteborn, F.C., Roush, T.L. and Cohen, M. (2000). Thermal Emission Spectroscopy of 1 Ceres: Evidence for olivine. In: M.L. Sitko, A.L. Sprague and D.K. Lynch (Eds.), Thermal Emission Spectroscopy and Analysis of Dust, Disks, and Regoliths (ASP Conf. Ser., vol. 196), Univ. of Chicago Press, Chicago, pp. 197-203.

8.6.3.9 Summary table

Table 13 Summary table of the mid-IR spectrometer

Parameter	**Units**	**Value/Description**	**Remarks**
Reference P/L	N/A	SMI	Spatially Modulated Interferometer
Spectral range	cm^{-1}	400 - 2000	
Spectral Range	μm	5 - 25	
Spectral resolution	cm^{-1}	10	
Optics			
Type of optics	N/A	Aspheric Al Mirrors, coated mid-IR beam splitter	
FOV	Degrees	9.2x6.9	Detector array FOV
Pixel IFOV	µrad	250	
Pixel IFOV	m	1.25m	At 5km range
Aperture	mm	100x100	Dependent on scan mirror geometry this is a minimum.
Focal length	mm	100	
Focal number	#	4	Indication only, the FOV is not circular
Detectors			
Type of detectors	N/A	Uncooled 640x480 micro bolometer array	ULIS baseline. Other candidate options possible
Pixel size	μm	25	Operating mode may combine pixels
Exposure time	sec	0.05	Integrated within instrument during normal operation

Signal to noise ratio		86 @ 300K	For 5m resolution, 1000cm^{-1} (10μm)
Physical			
Mass, total	kg	3.0 Kg	
Dimension	mm	160x220x370	
Volume	cm^3	13024	
Operating temperature	°C	-10C optimal	Can be controlled by a TEC, dependent on detector type used
Power			
Total average power	W	2	
Peak power	W	3.5	Hot calibration target
Data			
A/D conversion	bit/pixel	16	
Data volume	Mbyte	45	Per 5m resolution surface map
Data volume	Mbyte	450	For complete phase angle mapping of asteriod
Data volume	Mbyte	1500	Estimate for whole mission
Compression factor		2.5	Based on Cassini/CIRS

8.7 Radio Science Experiment - RSE

8.7.1 Introduction

The determination of asteroid masses is usually done by the observation of close approaches of nearby asteroids or for binary asteroids, by measuring the influence of the primary over the secondary. However, such situations are not common and this is why masses are not known for a great number of bodies. Knowing the mass is scientifically important because, accompanied with an accurate shape model, it allows the determination of the body's bulk density, which in turn gives some indication of its internal structure, such as the amount of porosity. Thus the accurate determination of the mass of the target is always considered as a high priority of space missions aimed at visiting a small body, even if it is not the ultimate mission objective.
Radio Science (RS) is the general study of phenomena affecting the propagation, scattering and reception of electromagnetic transmissions with wavelengths longer than roughly 0.1 mm. In the context of planetary science, this term has come to indicate a focus on the use of radio signals travelling between the spacecraft and an Earth terminal. It then includes the scientific application of radio tracking data for the precise determination of spacecraft's orbit and the scientific information that can be derived from such determination. Radio signals provide an extremely precise measurement of the radio path between the ground station and the spacecraft. When the radio path is well-clear of occulting material, the spacecraft can be treated as a "test particle" falling in the gravity field of the planetary system with the component of its velocity along the line-of-sight to the tracking station measured by the Doppler effect. Gravity experiments are based on determining the motion of the satellite in response to the variations in mass distribution within a planet, and this method has been extended to small bodies. See as an overview for Mars Express, Venus Express and Rosetta, the RS descriptions in Pätzold et al. (2004), Häusler et al. (2006) and Pätzold et al. (2007). The NASA Near probe used RSE to determine the mass of the asteroid Mathilde (Yemonans et al. 1997) and the gravity field of Eros (Yeomans et al., 2000).

The Radio Science Experiment (combined with data from the satellite's camera and possibly a Laser Altimeter) can thus determine the mass, centre of mass (as opposed to centre of figure), gravity field, shape, rotation axis and moments of inertia of the object. The motion of the satellite is monitored using Doppler shifts of the transmitted radio carrier frequency and solving for the gravitational field of the object, with knowledge of the relative position of the object and the satellite and the object's rotation state. If the distance to the object is sufficiently close and the observation duration is long enough, it can also allow the determination of the higher orders of the body's gravity field which is a key science objective to gain a first ideas of the internal structure of the body and the mass distribution relating to the surface shape. Indeed, the harmonic coefficients of the gravity field can be determined and compared with those expected from an object with the same shape but a uniform density distribution. Any differences would indicate some degree of large-scale inhomogeneity. All the retrieved parameters from the RSE will necessarily be solved for simultaneously based on data from a set of radio science passes. These passes

will need to have ground tracks well-distributed across the body's surface in order to sample the gravity field effectively. However, measuring anything more than J2 remains very challenging for small objects.
Mars Express has made the most precise mass determination of the Mars moon Phobos in July 2008 at a distance of 270 km (Andert et al., 2008). It turned out that not only the distance needs to be close but that also the geometry Earth/Mars/orbit plane needs to be optimal in order to receive the largest component of the change in flyby velocity along the line-of-sight. For the estimate of higher gravity field harmonics, the flyby distance needs to be within 100 km distance which shall be realized in 2010/11.

8.7.2 Scientific Goals and Performance Requirements

The following requirements are cited from the Science Requirements Document as reference for the expected scientific performance of this instrument;

GR-040: The mass of the NEA shall be determined with an accuracy of about 1 %..
AS-010: The inner structure of the NEA should be constrained, with the goal of doing this to a depth of about 100 m and a spatial resolution of about 10 m.
AS-020: The J2 terms of the gravitational field should be determined with an accuracy of 10 %.

Science requirement:
The accuracy of the mass determination increases obviously with the proximity of the object to the satellite. For the same accuracy, the level of required proximity depends on the mass of the object (less massive object need a closer approach). In the current concept, the satellite should fly closely to the asteroid and even land on it. Having an accurate knowledge of the mass is extremely important because, accompanied with an accurate shape model (volume) via imaging and laser altimetry, it can allow an accurate determination of the bulk density of the object. From experience, the mass determination is always much more precise than the volume determination therefore the error of the volume determination is the driver for the error in the mean bulk density. A mass determination with accuracy of 1% or less should nevertheless be considered.

Instrument requirements:
Radio Science instrumentation combines equipment on the ground with on-board spacecraft hardware required to create and maintain a highly stable and precise radio link. Two-way radio signals are generated on the ground and transmitted uplink through large ground station antennas. These signals are received by the spacecraft transponder, translated in frequency, and then retransmitted downlink to the Earth where they are received at the ground station antenna. The radio carrier frequency of the downlink signal is coherently related to the received uplink frequency by a fixed integer ratio. The downlink signal frequency is derived precisely from that of the uplink. Hydrogen maser clocks are used for the fundamental frequency reference on the ground, hence measurement of the downlink phase provides an extremely precise method for determining changes in the round trip propagation time to the spacecraft. For instance, a 1-Hertz difference between the frequencies of the uplink and downlink signals means that the total radio path length is

changing at the rate of 1 wavelength per second. Overall the short-term accuracy of the measurement procedure depends on the signal-to-noise ratio achieved and, ultimately, on the stability of the ground station oscillator over the round trip flight time of the radio signals to the spacecraft and back.

In general, the RSE experiment needs accurate information of the following parameters:

- Relative motion between Earth and asteroid
- Earth rotation
- Earth solid tides
- Propagation effects of the electromagnetic waves
- Non gravitational forces
- Spacecraft motions
- High Gain Atnenna (HGA) pointing motion
- Mechanical deformation of the onboard and ground antennas.

In order to extract the perturbation of the spacecraft motion caused by the body´s gravity field from the received Doppler shift, the Doppler shift of the unperturbed motion needs to be "predicted". A Radio Science Simulator (RSS) developed at the Institute of Spaceflight Engineering of the Universität der Bundeswehr in Munich allows the prediction of received radio carrier Doppler shifts based on the estimated unperturbed orbit of the spacecraft and considering all other gravitational and non-gravitational forces or effects acting on the spacecraft (see above). This is routinely applied to the radio science observations of Mars Express, Venus Express and Rosetta. The prediction is precise up to an offset of 10 mHz to 50 mHz compared to the received radio frequency at X-band of 8400 MHz.

Doppler noise is the limiting factor for mass determination. It is caused by a number of sub-factors which can be quantified by the so-called Allan variation. Among these factors are the instrumental noise sources (e.g. thermal, transponder quantisation, ground station), which account for a large part of the error. However, these errors can be greatly reduced by integrating over a long time.

Perturbing forces, especially those induced by the Solar Radiation Pressure (SRP) can have a very strong effect on the motion of the spacecraft about small bodies. The SRP forces quickly build up eccentricity and thus, within just a few days, lead to an impact or an escape from orbit. Numerical analysis has shown that the SRP helps maintain a sun-synchronous orbit. For a wide range of cross-section-to-mass ratios, the effect of continuous SRP forces on an orbit that is initially perpendicular to the Sun direction results in a rotation of the orbit plane, such that the near-terminator conditions are maintained, even for prolonged period. Thus, for the RSE to be successful, the SRP must be modelled accurately, and several studies have already developed such models. Non-gravitational forces can be difficult to characterize a priori because they require detailed modeling of the spacecraft geometry and surface properties, the attitude behaviour, the spatial and temporal variations of the incident radiation and particle fluxes and the interaction of these fluxes with the surfaces. These spacecraft models need to be an input for the RSS. The limitations on the accuracy are likely to be a result of varying SRP over the spacecraft surface. But the emission and absorption properties of the spacecraft surface materials must definitely be known with good accuracy (1% uncertainty at most).

During RS observations, thrusters operation must be avoided because of the great uncertainty in the associated forces and attitude changes. Attitude changes that do not use thrusters (i.e. using wheels) are allowed but will result in small changes that can be modelled in the perturbations due to the different geometry with respect to the Sun.

Solar plasma noise has also to be determined if signals go through regions of high-solar plasma density. The latter effect can be eliminated by using two radio links, for instance S and X-band or X and Ka-band. The use of two bands or VLBI techniques (Delta-DOR) may also be considered to eliminate the Doppler noise generated by ionospheric/tropospheric effects. A second larger downlink frequency allows not only the correction for the plasma noise but gives also a typically four times larger Doppler signal caused by the perturbed motion.

Based on experience and simulations, an observation campaign of 4 to 6 weeks after entering in the Hill's sphere of RSE tracking should allow a complete mapping of the gravity field of the object. However, this largely depends on the asteroid properties (mass, rotation rate, diameter). Moreover, all indications above depend on the chosen orbit (orbit plane angle with respect to Earth LOS, eclipse/no eclipse, etc …). Therefore, the precise definition of the RS requirements should be done once the orbital parameters are done.

8.7.3 Description

8.7.3.1 Instrument concept

No extra hardware is provided by the experiment team, the observations are done by using the on-board radio subsystem which consists of

- Transponder (redundant)
- Amplifiers (to be specified by the idustry for mission requirements)
- Radio Frequency Distribution Unit (RFDU) which connects all (redundant) receivers and transmitters at various frequencies with the available antennas
- High Gain Antenna (size to be specified in order to meet required to link budgets)
- Low Gain Antennas for near-earth phases after launch or emergency operations

The operational radio link is a two-way coherent radio X/X (baseline) and X/Ka (optional) link. A hydrogen maser in the ground station is used as the frequency standard for generation/reception of the uplink/downlink signal. A transponder system at the following frequency bands shall be used:

- X/X for spacescraft operations and communications; first radio science frquency band

- X/Ka optional for an improved Doppler signal by a factor of four compared to X/X and for the correction of the plasma noise in combination with X/X; second radio science frequency band

The following receiving and transmitting frequencies are common:

- X-band uplink (at approx. 7100 MHz)
- X-band downlink (at approx. 8400 MHz)
- Ka-band downlink (at approx. 32000 MHz)

The satellite radio subsystem shall then be capable of using a transponder for the X/X or X/Ka-band for both RSE and spacecraft operations and communications.
The transponder ratios of the coherent radio links shall be constant with the following numerical values:

- X-band transponder ratio: k_X = 880/749
- Ka-band transponder ratio: k_{Ka} = 3344/749

for the X-band uplink in the 7100 MHz frequency band.

The radio link shall be capable of guaranteeing the required Doppler and range errors for worst case conditions (rain attenuation) assuming 95% availability. The ranging tone frequency of 25 MHz should be the baseline. Other advanced techniques (Delta DOR measurement via VLBI technique) may also be considered as an option.

The radiofrequency subsystem shall be able to operate all links simultaneously via the High Gain Antenna (HGA). Depending on the mission design and in particular the geometry between the Sun, Satellite, the Earth and the object, a steering antenna or some agile capability (3-axis active control) may be required.

8.7.3.2 Orbit, operations and pointing requirements

Orbit

The RSE orbit must be chosen so that it can achieve the requirements defined in previous sections. The length of the observation campaign depends on many factors concerning the asteroid properties (e.g. true rotation period of the object) and both the length of a tracking pass and the number of tracking passes per day.

Operations

The satellite shall not perform AOCS (Attitude and Orbit Control System) operations during four consecutive operation windows. Possible operation constraints shall be clearly identified. The High Gain Atenna (HGA) shall be pointed toward the Earth and the spacecraft shall have a permanent communication link with the ground segment during RSE operations. The satellite radio subsystem shall then be capable of using a transponder for the X/Ka-band for both RSE and spacecraft operations and communications. It shall then be able to operate all links simultaneously via the High Gain Antenna (HGA).

Pointing

The HGA pointing accuracy (or spacecraft if no antenna pointing system) shall be greater or equal to 0.1 times the 3dB beam width during the whole time of RSE operations. The pointing stability of the system shall be such that the residual velocity error is smaller than 0.1 μm/s at all times during RSE operations.

8.7.3.3 Interfaces and physical resource requirements

Thermal control
The RF system is sensitive to temperature variations. It should then be located in a thermally stable environment of the spacecraft in order to avoid thermal insulation. The heat dissipated by the RF signal generation is about 5 W so no active thermal control system is required.

Electronics, radiation shielding
No particular radiation shielding is required. Most needed components of RSE equipment are or will be flight proven in a near future (Smart-1 and Bepi Colombo).

Data processing and transfer
The basic amount of data from an RSE is very low and is limited to house keeping data. However, f the RSE is combined with camera and laser altimeter measurements to determine the 3D-shape model of the object, advanced algorithm shall be necessary and the data processing loads shall likely be needed.

Mechanical structure and hardness
No particular stability requirements are needed.

Power
The KaTe experiment on Smart-1 had a power consumption of 18 W. Deep Space 1 carried a similar transponder having a peak consumption of 13 W. Thus, 15 W seems a reasonable value, taking into account technology improvements in the frame of Bepi Colombo.

Mass
Most of the equipments are part of the telecommunication subsystem and are therefore not considered as payload equipment. However, the upgrade of the telecommunication X/X transponder to also be able to use X/Ka downlink band implies additional mass and power with subsequent modification of the antenna. This capability is beneficial for scientific reasons in order to enhance the Doppler perturbation signal by the gravity field by a factor of four compared to X/X and in order to correct for the plasma noise contribution. As an indication, the mass of the experiment KaTe onboard SMART-1 was 4.7 kg, for a 18 W X/Ka band transponder. The mass of a classical X/X band transponder (see, e.g., Hershel) is about 3 kg. Therefore, the additional mass may be about 1.5 kg, assuming some technology improvements.

8.7.3.4 Calibration

The estimate of the accelerations due to SRP relies on the knowledge of the optical properties of the spacecraft surfaces (emissivity, absortivity and reflectivity). To achieve the required accuracy, these properties shall be known to an accuracy of 1% at the beginning of the gravity campaign and 10% at EOL.

8.7.3.5 Cleanliness, ground activity and other requirements

A complete error budget of the measurements will necessarily include the ground system and ancillary instrumentation. This is especially important as the mechanical noise of the antenna and tropospheric noise will be the leasing sources of measurement errors in range rate. While little can be done to limit the antenna mechanical noise (gravity and wind loading), tropospheric noise, mostly due to water vapour, can be successfully calibrated by means of advanced water vapour radiometers. The need for these calibration instruments shall be carefully evaluated.

The ground segment shall be selected to be adapted to the requirements described in previous sections. In particular, it shall be capable of:

- Transmitting an X-band uplink carrier signal modulated with TC and range signals.
- Receiving X-band and Ka-band (if implemented) downlinks simultaneously.
- Receiving dual frequency ranging signals.

These requirements are more or less already implemented in ESA´s Cerbreros ground station and in most NASA DSN ground stations.

The timing error of the maser clock, NCO phase readout accuracy and path delay instabilities shall then be limited to reduce the resulting error contribution to the 1-sigma Doppler and Ranging noises. The use of a second station may also be considered to reduce the time needed for the determination of the gravity field.

8.7.3.6 Critical points

As indicated, many aspects of the RSE need some crucial mission parameters to be evaluated against the achievement of the scientific goals. The most important ones are the mass of the target asteroid, the orbital distance and the measurement time. The mass and the orbital distance affect the determination of the gravity field, the asteroid centre of mass and the spacecraft position from the asteroid. A larger mass would be desirable in order to increase the determination of these parameters. However, potential targets for a space mission are generally small (below a few km in size) so the RSE will be necessarily done in a low-gravity environment. A smaller orbital distance from the asteroid would be desirable in order to help the positioning of the spacecraft with respect to the center of mass. A trade off evaluation of these parameters is surely needed. The same holds true to concerning the parameters which will help size the system. These concern the requirements on Allan variance (propagation media, thermal and mechanical deformation, station location, uncertainty of the HGA motion about the spacecraft center of mass, thermo-mechanical stability of the HGA etc ...), the radio link budget to reach the required SNR (atmospheric loss, rain attenuation link, antenna gains, downlink/uplink power, noise temperature, etc ...).

Finally it has to be noted that the RSE will not allow by itself the investigations of the interior properties deep into the object. Indeed, as it was demonstrated by the analysis of RS from the NEAR mission (Miller et al. 2002), there is no unique solution for the mass distribution. Radio reflection tomography or seismic experiments would be required to better discriminate between a rubble pile or a monolithic body, which would be of high scientific interest.

8.7.3.7 Analysis of achievable accuracy by ESOC

The analysis by Jehn and Timm 2009 demonstrate to what accuracy with dependence on the orbital distance the asteroid's mass and J2 term can be achieved;
It is well known that a better knowledge of the gravity coefficients can be achieved if the spacecraft orbits the asteroid at lower altitudes. In this section an orbital radius of 5 asteroid radii is assumed which corresponds to a semi-major axis of 2.45 km. This orbit is not stable as Figure 13 shows. After 30 days the eccentricity will grow to 0.5 and after 40 days the pericentre altitude reaches the surface of the asteroid.
Figure 14 shows what level of uncertainty can be reached in such a low orbit. After 30 days, the mass will be known by 3.6 %, the J2 by 4.8 % and C22 by 6.0 %.

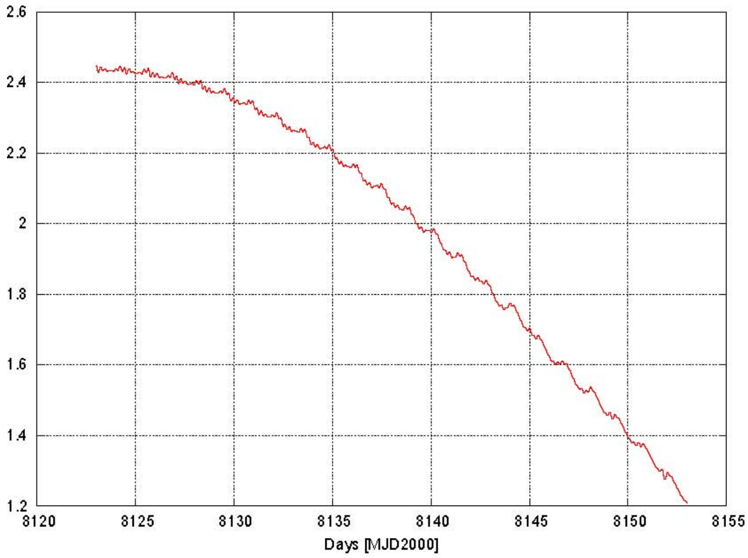

Figure 13 Pericenter radius evolution for a low initial orbit of 5 asteroid radii.

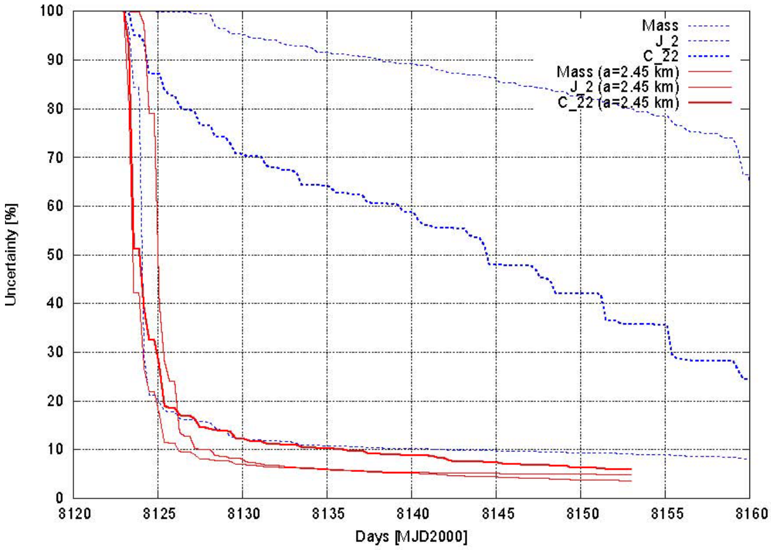

Figure 14 Knowledge of the mass and of the gravity coefficients C_{20} *and* C_{22} *for an initial orbital altitude of 10 asteroid radii (baseline) and of 5 asteroid radii (a= 2.45 km).*

In a more refined analysis it is assumed that the spacecraft stays 30 days in the 10 asteroid radii orbit before it is re-orbited into a circular orbit with an altitude of 2.5 km where it shall stay another 30 days. Every 10 days the eccentricity is put back to nearly 0 by a pericentre raise and an apocentre lowering manoeuvre. It is assumed that these manoeuvres are performed instantaneously, however in real operations a few days will be spent for each orbit change during which no science is possible. Therefore to achieve the results as shown below, 70 rather than 60 days will be required in total.
The orbital element of the spacecraft at the beginning and end of each orbit leg are given in Table 14.

Table 14 Orbital elements (in a Mean Earth Equator 2000 system) of Marco Polo before and after the orbit manoeuvres

Leg 1	Epoch (MJD) 8123	Semi-major axis (km) 4.895	Eccentricity (-) 0.988E-3	Inclination (deg) 69.570	RAAN (deg) 162.212	Arg. of Peri-centre (deg) 271.100	True Anomaly (deg) 180.0
	8153	4.929	0.421	71.259	186.313	265.341	154.304
2	8153	2.500	1.000E-5	71.259	186.313	265.341	154.304
	8163	2.471	0.173	74.224	186.212	273.244	-139.402
3	8163	2.500	1.000E-5	74.224	186.212	273.244	-139.402
	8173	2.487	0.262	76.846	186.765	274.076	-125.169
4	8173	2.500	1.000E-5	76.846	186.765	274.076	-125.169
	8183	2.485	0.331	79.567	187.733	271.412	-127.679

The current GRETCHEN software can only be run with the same initial uncertainty in all gravity coefficients of the same degree. After the first leg of the trajectory the C22 is much better determined than the J2, but since both are of degree 2, the simulation of the next trajectory leg has to start with the same uncertainty for both coefficients. To be conservative the worse knowledge (i.e. the one of J2) is chosen. This explains the feature in

Fig. 14 where the knowledge of C22 deteriorates from 36 % to 82 % on day 8153. However, this software constraint has only a marginal effect on the final results, because the uncertainty drops so quickly in the lower 2.5 km orbit, that the initial uncertainty plays a minor role. Fig. 14 shows the level of uncertainty that can be reached after 60 days: the mass will be known by 2.1 %, the J2 by 5.1 % and C22 by 4.8 %.

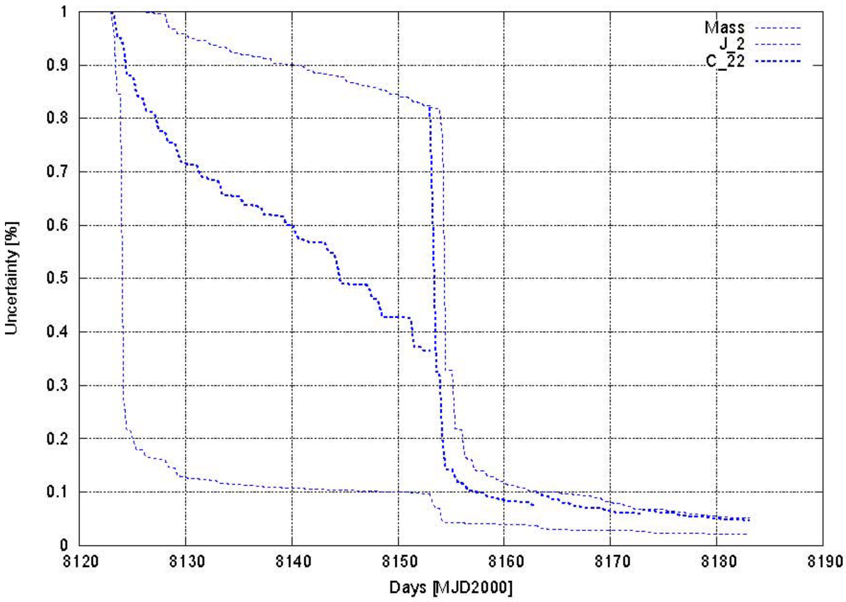

Figure 15 Knowledge of the mass and of the gravity and of the gravity coefficients C_{20} and C_{22} when the spacecraft stays 30 days in a high (10 asteroid radii) orbit and 30 days in a low (2.5 km) orbit. The knowledge of C_{22} has jumps due to software artefacts (see text)

Furthermore the report (Jehn and Timm 2009) summarises options to which extend the analysis can be refined.

In the baseline configuration of Marco Polo (see Chapter 2.6 for a summary of the assumptions) the asteroid mass can be estimated with a precision of about 3 %. The gravity coefficient C22 can be determined with a precision of 12 % if 180 days of range and Doppler data is analysed. The J2 term is even more difficult to determine: an uncertainty of 26.7 % will remain.

Better results can be achieved if a multi-frequency link including Ka-band (as foreseen with BepiColombo) will be used instead of a single X-band up- and down-link. In this case the Doppler noise can be reduced to 2.5 µm/s and the J2 and C22 can be determined with a precion of 11.3 and 2.9 %, respectively. However, the precision of the mass estimate will not improve very much. It will remain at about 2 % even if the station location uncertainties are reduced by a factor of two.

Another option is to lower the orbiting altitude. If the semi-major axis is reduced from 10 to 5 asteroid radii after 30 days and the orbit is maintained nearly circular at this altitude for another 30 days the mass will be known by 2.1 %, the J2 by 5.1 % and C22 by 4.8 %.

8.7.3.8 Heritage

The NEAR Shoemaker spacecraft performed a RSE campaign on the asteroid Eros and reached accuracies of 0.04% and 1% on Eros' mass and volume, respectively, with an X-band coherent communication system. The antenna was non-gimballed. The spacecraft orbited the asteroid during one year. Note that Eros's mean diameter is about 16 km (it is the second largest NEO after the 40 km-size Ganymed) so it is much larger (more massive) than potential future NEO targets.

Mars Express determined the mass of Phobos at a precision of 0.08% at one close flyby at 270 km in July 2008 (Andert et al., 2008).

The Rosetta satellite also carries a RSE which will fulfil the requirements. It is equipped with a dual X-band and S-band telecommunication system and has large flexibility through a steering antenna. It also has an Ultra Stable Oscillator for the accurate referencing of the one-way signal. Note that the target of Rosetta is an active comet, so that outgasing activities may occur during the campaign. It has been estimated that the mass of the comet nucleus may be determined to a precision of less than 0.1% (Pätzold et al., 2001a). The precision of the mass determination of the Lutetia asteroid at a distance of 3000 km by Rosetta in July 2010 is estimated to less than 4% (Pätzold & Andert, 2009).

Bepi Colombo and the Don Quijotte concept are based on the same architecture as Cassini, i.e. carrying a dual X/Ka uplink/downlink RSE system. The results of the Cassini radio science experiments and the analysis carried out for the experiment MORE of the mission BepiColombo to Mercury clearly indicate that only a multifrequency link in its full configuration can provide the best observables (range and Doppler) over the long time scales of the experiment. Note that a potential target of the Don Quijotte concept was the D-type NEO 2002 AT4, whose size is below 1 km, and that the RSE was the main tool of the mission for the measurement of the mass and the deflection of the object by an artificial projectile. Building on the ongoing development of these two missions is certainly the best strategy. The X/Ka-band approach should then be adopted, as it is less sensitive than the S-band to plasma effects (but more sensitive to weather effects). However, the required level of accuracy does not need to have a Ka-band uplink and thus, a Ka/Ka transponder does not have to be considered.

Smart-1 also demonstrated in Europe the use of the Ka-band downlink through the experiment KaTe. This experiment can be reused in this frame and would be the most suitable for the considered application, with a total mass of 4.7 kg, consistent with the required mass budget. Ongoing development in the Bepi Colombo framework should also be taken into account to increase the performances. An X/Ka-band transponder (strictly similar as the one needed) has also been developed by Motorola and JPL and has flown onboard Deep Space 1 with a mass of 3 kg and a power consumption of 13 W.

1.1.3.8. References

Andert, T.P., M. Pätzold, B. Häusler, Direct measurement of the mass of Phobos with the radio Science experiment MaRS onboard Mars Express, paper presented at the EGU General Assembly 2008, Vienna, Austria, 2008.

Häusler, B., M. Pätzold, and 11 Co-Authors, Radio science investigations by VeRa onboard the Venus Express spacecraft, Planet. Space Sci., 54, 1315-1354, 2006.

Jehn and Timm, 2009, MAS Technical Note No. 75, SRE-PA/2009.023/MarcoPolo, Issue 1.1, Gravity Field Estimation of 1999 JU3 with MarcoPolo.

Miller, J. K., Konopliv, A. S., Antreasian, P. G., Bordi, J. J., Chesley, S., Helfrich, C. E., Owen, W. M., Wang, T. C., Williams, B. G., Yeomans, D. K. and Scheeres, D. J. 2002. Determination of Shape, Gravity, and Rotational State of Asteroid 433 Eros. Icarus 155, 3-17.

Pätzold, M.; Häusler, B.; Wennmacher, A.; Aksnes, K.; Anderson, J. D.; Asmar, S. W.; Barriot, J.-P.; Boehnhardt, H.; Eidel, W.; Neubauer, F. M.; Olsen, O.; Schmitt, J.; Schwinger, J. and Thomas, N., Gravity determination of a comet nucleus: Rosetta at P/Wirtanen, *Astron. Astrophys. 375*, 651-660, 2001a.

Pätzold M. et al., MaRS: Mars Express Orbiter Radio Science, In: Mars Express: the scientific payload. Ed. by Andrew Wilson, scientific coordination: Agustin Chicarro. ESA SP-1240, Noordwijk, Netherlands: ESA Publications Division, ISBN 92-9092-556-6, p. 141 – 163, 2004.

Pätzold, M. et al., Rosetta Radio Science Investigations, *Space Sci. Rev.* 128, 599, 2007.

Pätzold, M. and T. Andert, Rosetta/Lutetia flyby: Feasibility of asteroid mass determination, ROS-RIU-TN-3130, 2009.

Yeomans, D. K., Barriot, J.-P., Dunham, D. W., Farquhar, R. W., Giorgini, J. D., Helfrich, C. E., Konopliv, A. S., McAdams, J. V., Miller, J. K., Owen, W. M., Jr. , Scheeres, D. J., Synnott, S. P. and Williams, B. G. 1997. Estimating the Mass of Asteroid 253 Mathilde from Tracking Data During the NEAR Flyby. Science 278, 2106.

Yeomans, D. K., Antreasian, P. G., J.-P., B., Chesley, S. R., Dunham, D. W., Farquhar, R. W., Giorgini, J.D., Helfrich, C. E., Konopliv, A. S., McAdams, J. V., Miller, J. K., Owen, W. M. J., Scheeres, D. J., Thomas, P. C., Veverka, J. and Williams, B. G. 2000. Radio science results during the NEAR- Shoemaker spacecraft rendezvous with Eros. Science 289, 2085-2088.

1.1.3.9. Summary Table RSE

Table 15 Example of a summary table of technical features of the radio science experiment

PARAMETERS	Units	Value	Remarks
			Most of characteristics are TBC in the course of the study
GENERAL			
Instrument name		NEARSE	NEA-Radio Science Exp
Heritage		SMART-1, Bepi Colombo, Don Quijote	
Reference P/L		KaTe, BC/DQ RSE	
Type of instrument		Transponder	
Function mode		Range rate and rate measurements	
REQUIREMENTS			
Ranging tone frequency	MHz	25	
X uplink frequency	MHz	7200	
X downlink frequency	MHz	8400	
Ka downlink frequency	MHz	32500	
(Or S downlink frequency)	(MHz)	2300	
Instrumental Doppler shift $\sigma_v(t)$	m/s	1.10^{-7}	Over 10^4 s
Frequency readout interval	s	1	At ground station
Ranging accuracy	ns	TBD	
ALLAN VARIANCE			
Total	NA	$<10^{-15}$	At 10^3 -10^4 s integration time
Individual contributors	NA	TBD for all contributors (propagation media, ground system, spacecraft)	
DATA RATES/VOLUME			
Data rate	kbps	~0.1	Housekeeping only (Mostly taken into account in telecommunication budget)
OPERATIONS			
Operational time	weeks	mini. 6 weeks campaign	
Orbit	NA	Preferrably low altitude for better determination of gravitational field	
POINTING AND ALIGNMENT			
Pointing control	arcmin	0.1 times the 3dB beam	To limit losses in the Link budget
Pointing stability	arcsec/s	TBD	
THERMAL			
Operating temperature range	°C	-20 ; +60	
Non-operating temperature range	°C	-40 ; +75	
POWER			
Total average power	W	TBD	
Power peak	W	15	The power consumption of the Ka band downlink of Bepi Colombo is 9 W (Since highest powed peak is given by Ka band, it must be taken into account as payload power budget)
PHYSICAL			
Units	NA	1	Only X/Ka transponder considered as payload
Preferred location	NA	No specific requirement	
Mass, total	kg	1.5	This is the mass of the extra equipment needed to account for the Ka downlink. The mass of the regular X/X band transponder can be taken into account in the telecommunication budget as being 3 kg
Location	NA	Thermally stable location	For link stability
CLEANLINESS AND OTHERS			
EMC requirements		Standard	
Chemical		None	
Vibration	g	25 rms random	
Shock	g	100	
Mechanisms	NA	None	

8.8 Neutral Particle Analyser

8.8.1 Introduction

The surface properties of a NEO and its interactions with solar wind are the scientific targets through which important information about surface evolution and, finally, about the global evolution history of the body. In particular, this investigation will answer one of the main questions of the Marco Polo NEO Sample Return mission: "What processes can be identified as happening on the surface of these small airless bodies as a result of exposure to the space environment and collisions?"

The asteroid is eroded by different processes (such as solar wind, and solar and cosmic ray bombardment and by micrometeoroid impact vaporization) and its superficial composition is modified by this space weathering and gardening (Hapke, 2001). The particles released from the body's surface are essentially lost in space since the escape velocity is very low. The relevant surface release processes at these distances from the Sun are Photon Stimulated Desorption (PSD), Ion-Sputtering (IS) and Micrometeoroid Impact Vaporization (MIV). The mean surface temperature is low; hence, the surface erosion due to the thermal desorption (TD), relevant only at Sun distances lower than 1 AU (Plainaki et al., 2009), is negligible.

Observations of the gas expanding from the asteroids are of crucial importance to identify and to localize the physical processes acting onto the surface as well as to estimate their efficiencies. In particular the ion sputtering is one of the most important processes causing alteration and erosion of the surface.

The key questions of NPA are summarized as in the following:

1. What processes can be identified as happening on the surface of the NEO as a result of exposure to the space environment and collisions? What is the erosion and the space weathering significance at the NEO surface?
2. What is the efficiency of each process as a function of environment conditions?
3. Is the efficiency of particle release processes uniform in the NEO surface?
4. What is the composition of the escaping material and consequently, how it relates to the surface composition?
5. What is the role of the surface release processes in the body evolution?

8.8.2 Scientific Goals and Performance Requirements

The NPA scientific objectives are:

1. To identify the particle release processes active on the NEO surface
2. To evaluate the efficiency of each process as a function of environment conditions
3. To evaluate the efficiency of each process as a function of surface properties
4. To determine the composition of the escaping material
5. To estimate the role of the surface release processes in the body evolution.

8.8.2.1 Estimated neutral atom signal

Ion-sputtering and other surface release processes at NEO

The expected signal needs to be carefully evaluated considering each surface release process

Ion-sputtering results from the impinging of an ion of mass m_1 onto a surface; if the impact energy (E_i) is high enough, a new particle (m_2) may be extracted. In most cases, the ejected particle is neutral (Hofer, 1991). The energy transmitted in the collision is:

$$T = T_m \cos^2(\alpha_r)$$
$$T_m = E_i \frac{4 m_1 m_2}{(m_1 + m_2)^2}, \qquad (1)$$

where T is the transmitted energy, T_m is the maximum transmitted energy and α_r is the recoil angle of the ion. The distribution function (f_S) of the ejection energy has been empirically obtained (*Sigmund,* 1969; *Thompson* 1968); the results are reproduced by the following function:

$$f_S(E_e, E_i') = c_n \frac{E_e}{(E_e + E_b)^3} \left[1 - \left(\frac{E_e + E_b}{T_m}\right)^{\frac{1}{2}}\right], \qquad (2)$$

where E_b is the surface binding energy of the atomic species extracted, E_e is the energy of emitted particles, c_n is a normalization constant.

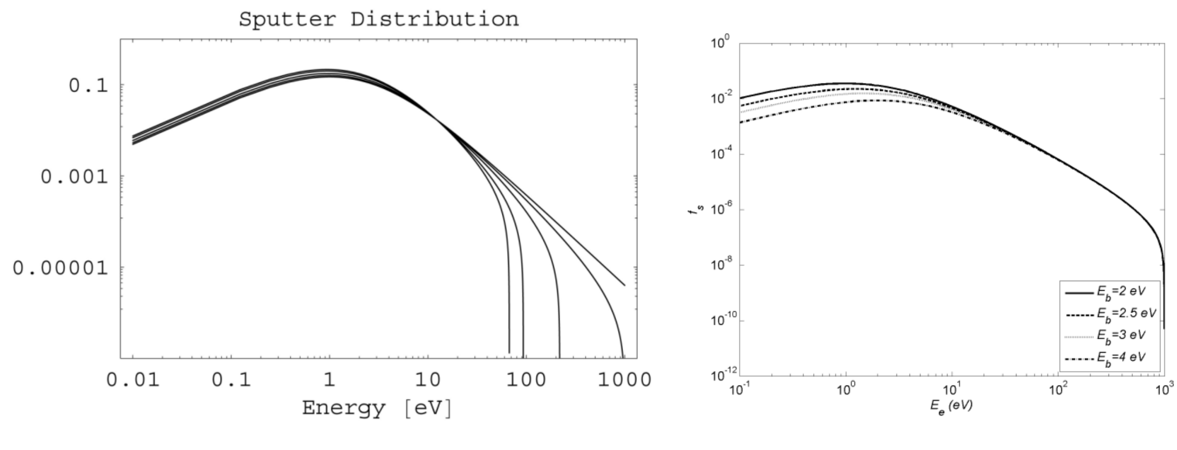

Figure 16. Solar wind sputtering normalized energy distribution function (left) for different species (Fe, Ca, Na, O, H) and (right) for different binding energies from a regolith.

The normalized energy distribution function for different species and different binding energies, assumes different profiles; anyway, generally it peaks at few eV but extends up to hundreds of eV (Figure 16).

The other surface release processes acting on the NEO are not able to eject particles at energies above few eVs; hence, the detection of particles above 10 eVs is a method to identify the action of the ion-sputtering process.

Plainaki et al. (2009) simulated the sputtered particles from a NEO. They considered a solar wind proton flux of $\varphi_{H+}=10^{12}$ $m^{-2}s^{-1}$ as the total amount of the impinging particles.

The NEO radius was assumed to be 0.5 km; its mass was taken as 10^{12} kg. Different kinds of NEO surfaces produce some differences in the yield of the process and, hence, in the total released flux (Hapke and Cassidy, 1978). A similar study has been performed by Schläppi et al. (2008) for the asteroids (2867) Steins and (21) Lutetia in preparation of the upcoming Rosetta flybys. Plainaki et al. (2009) considered three different cases of carbonaceous chondrites comprising the actual body of the near Earth object: CI, CM, Tagish-Lake types. The bulk abundances of the main elements constituting each one of the above mentioned categories are presented in Table 16.

Table 16: Bulk element abundances for CI-chondrites, CM-chondrites and Tagish Lake type chondrites (adapted from Brown et al., *2000).*

Mass (amu)	Element	CI (atoms%)	CM (atoms%)	Tagish Lake (atoms%)
1	H	55	45	47
12/13	C	8	6	9
24/25/26	Mg	11	15	14
27	Al	1	1	1
28/29/30	Si	10	15	13
32/31	S	4	3	3
40/44	Ca	1	1	1
54/**56**/57	Fe	9	13	11
58/60/59	Ni	1	1	1
	Total	100	100	100

A summary of the input parameters used by Plainaki et al. (2009) is presented in Table 17.

Table 17: Input Parameters describing NEO environment

Parameter name	Symbol	Suggested Value
Solar-wind flux	φ_{H+}	10^{12} m^{-2}s^{-1}
Energy of the incident particle	E_i	1000 eV
Mass of the incident particle	m_1	1 AMU (proton)
NEO Radius	R_{NEO}	500 m
NEO Mass	M_{NEO}	10^{12} kg
Average sputtering yield	Y	0.05
Binding energy	E_b	2 eV

According to the simulations (Plainaki et al. 2009), for the case of a NEO surface consisting of CI type chondrites, significantly higher fluxes of neutral sputtered particles (up to 10^{11} particles m^{-2} s^{-1}) appear in a region extending from the NEO surface up to an altitude of about 1 km (Figure 17, left). Because MarcoPolo will perform a NEO a local characterization at a distance of about 1 km, the NPA instrument will have a good possibility of recording significant fluxes of sputtered particles. According to the right panel of Figure 17 the derived total emitted particle density is sufficiently big, reaching the value of about $10^{6.5}$ particles m^{-3} near the NEO surface. This result is in good agreement with the calculations made by Scläppi et al. (2008) for asteroids Lutetia at a distance of about 2.72 A.U, and Steins at 2.14 AU.

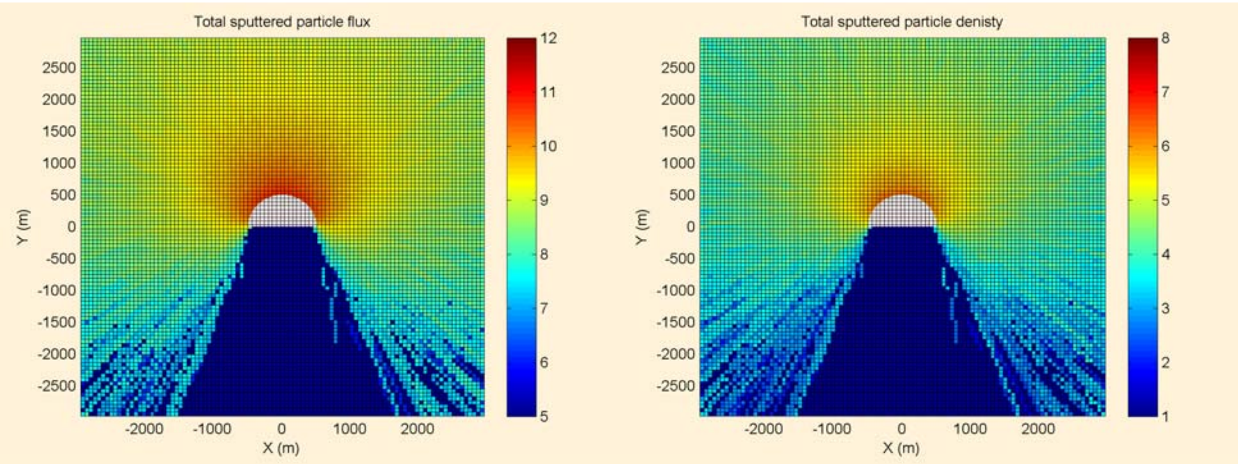

Figure 17**:** Sputtered particle flux (in logarithm of particles m-2 s-1, left) and density (in particles logarithm of m-3, right) distributions for impinging particle of energy ~1000 eV. The NEO surface is assumed to be consisting of CI chondrites (Plainaki et al. 2009).

PSD and TD contribute to the total released particle density emerging from the NEO surface. Especially for volatile elements like H and C, since it constitutes a process that regards exclusively volatile species. The results of Plainaki et al. (2009) simulations show that the total density of the volatiles emerging from the NEO surface, via the PSD process, is ~ $1 \cdot 10^8$ particles/m^3. Moreover, a rough estimation of the particles emerging via TD for different values of the surface temperature *T* results in values from ~10^4 particles/m^3 (for *T*=400K) to ~$5 \cdot 10^8$ particles/m^3 (for *T*=500K). Summarizing the results from simulating both PSD and TD, the total released particle density varies from ~ $1 \cdot 10^8$ particles/m^3 to ~ $6 \cdot 10^8$ particles/m^3. This value is in agreement to that calculated by Schläppi et al (2008) for asteroid Steins (~ $2 \cdot 10^8$ particles/m^3), at a distance of about 2.72 A.U. The fluxes emerging via the processes of PSD and TD are 1.5-2 orders of magnitude more intense than those emerging via solar-wind sputtering for volatiles at low energies. Other processes (like MIV) should be considered especially for refractories. Nevertheless, the higher energy released particles originate only via ion-sputtering (Milillo et al., 2005).The simulation considers an average solar wind condition. In the case of solar extreme event activity a major released flux is expected.

Plainaki et al. (2009) showed that the most important contribution to the total sputtered particle flux comes from the H particles emitted (about 90% of total flux). This is due to the big H relative atom composition, because of the low H atom mass.

The differences between the considered cases of CM and CI chondrite-type NEO surfaces are more distinguishable in the regions near the NEO surface.

The particles at energy E_e>10 eV (Sputtered High-Energy Atoms- SHEA) are about 1% of the total. If the orbiter will be at a distance of less than 1 km from a target with radius ~0.5 km, the estimated flux of high energy (above 10 eV) particles is $10^{8.5}$ $m^{-2}s^{-1}$.

8.8.2.2 Scientific requirements

The detection of released particles will provide a unique opportunity to estimate the loss rate from the NEO. The bulk of the surface released particles is in the illuminated side below the eV range and hence, the day-side measurement of the gas density will provide information about the intensity and the mass of emitted material. The identification of the mass of the released particles will give some hints on the NEO surface composition. It is likely that the radiation pressure action pushes some species toward the night side, forming a faint comet-like tail. Hence, the density measurements should be performed in the night side, as well

Nevertheless, different release processes are active on the NEO surface and, when only gas density is measured, it is difficult, if not impossible, to discriminate their different contributions or to reconstruct the emission regions on the surface (and derive areas with different release efficiencies). In fact, it is not possible to investigate whether the IS process is active without a measurement of the energy (or velocity) spectra, since this is the only process that releases particles at energies above 10 eV.

Moreover, a good angular resolution is important to identify the regions more active in releasing SHEA, thus evidencing possible anisotropies of solar-wind sputtering and/or of surface properties.

A comparison between simultaneous ion fluxes measured at the vicinity of the Earth and SHEA fluxes emitted from a NEO will provide an indication of the regolith efficiency in releasing material when exposed to solar wind.

Finally, in this way investigation of the alteration and erosion of the surface, in other words, space weathering activity, will be possible through remote sensing.

The ion sputtering and all the processes acting on the NEO surface will be even more investigated thanks to joint analysis of data from other payload instrumentation on board the Marco Polo mission that provides the remote-sensing of the surface properties (like V + NIR + MIR spectrometers and camera). In fact, additional information of the surface structure, mineralogy and composition will add constraints to model the release processes. Once the returned sample will be analyzed, even more detailed information will be achieved to be added to the RAMON data analysis. In fact Marco Polo will provide, for the first time, the opportunity to have in situ observations of the released particles together with detailed laboratory information on the mineralogy and composition of the emitting surface.

The following requirement is cited from the Science Requirements Document as reference for the expected scientific performance of this instrument;

GR-070: The flux, speed, direction and mass of atomic/molecular particles escaping from the surface should be measured to detect products of solar wind sputtering or other active release processes. The energy range from 0.01 to 1 keV shall be covered with an energy resolution of about 25 % and an angular resolution of 5° x 5°; the particles with energies <0.01 keV shall be measured with m/Δm of about 50.

LR-030: (As GR-070) The flux, speed, direction and mass of atomic/molecular particles escaping from the surface should be measured. The energy range from 0.01 to 1 keV shall be covered with an energy resolution of about 25 % and spatial resolution at surface about 10 m; the particles at energy <0.01 keV shall be measured with m/Δm of about 50.

In Table 18 the summary of NPA scientific performance requirements for each scientific objective is given:

Table 18: Summary of NPA scientific performance requirements. Red related to gas density measurements and blue related to SHEA detection.

Scientific Topic	Signal Intensity	Energy Energy resolution	Major Components	Angular FOV Angular resolution	Time resolution (s)	Observable region	Useful associated observations
1. particle release processes identification	10^2 cm^{-3}	< 1 eV Not req.	H, C, Mg, Si, S, Fe, others	- Not req.	60	Mainly dayside	
	10^4 cm^{-2} s^{-1} (for energy >10 eV)	>10 eV 25%	H, and refractories	5°x30° 5°x5°	60	dayside	
2. ion sputtering efficiency versus environment conditions	10^4 cm^{-2} s^{-1}	>10 eV Not req.	H, and refractories	5°x30° 5°x5°	60	dayside	Solar wind fluxes
3. ion sputtering efficiency versus surface properties	10^4 cm^{-2} s^{-1}	>10 eV 25%	H, and refractories	5°x30° 5°x2°	60	dayside	V+NIR+MIR +camera observations
4.gas composition	10^2 cm^{-3}	< 1 eV Not req.	H, C, Mg, Si, S, Fe, others	- Not req.	300	Mainly dayside But also nigh side	
5. role of surface release processes in the evolution	10^2 cm^{-3}	< 1 eV Not req.	H, C, Mg, Si, S, Fe, others	- Not req.	300	Mainly dayside	
	10^4 cm^{-2} s^{-1} (for energy >10 eV)	>10 eV Not req.	H, and refractories	5°x30° Not req.	300	dayside	

8.8.3 Instrument description

8.8.3.1 Neutral Particle Analyser required parameters

The estimation of the loss rate from NEO is accomplished by a Neutral Particle Analyser (NPA) able to resolve intensity, velocity and direction of the released particle flux. It is important to be able to cover the energy range up to hundreds of eV down to thermal energies in order to detect the products of all the active release processes.
In order to cover the whole energy range two sensors should be included in a single instrument design.
Required sensor characteristics
First sensor:

Energy range/resolution: <few eVs / no energy resolution
Mass resolution M/ΔM: about 50
Angular FOV/resolution: 5°x30°/ no angular resolution
Second sensor:
Energy range/resolution: 10-1000 eV / 25%
Angular FOV/resolution: 5°x30°/5°x5°
Mass resolution: no mass resolution
Time resolution: ~1 minute

8.8.3.2 Instrument concept

Detecting and characterizing neutral atoms in the energy range of interest, < 1 eV ÷ 1.0 keV, in an environment of photon, electron and ion fluxes, require 1) highly effective suppression of photons, electrons, ions and 2) two sensors for mass analysis and for velocity/direction analysis (particles above 10 eV).
The incoming radiation made by neutrals, ions and photons impinges upon an aperture. The ions and electrons are deflected by electrostatic lens before the entrance. The neutral particles pass through an entrance of about 1 cm^2 divided for detecting low energies and higher energies.
For low-energy particles detection and mass analysis, the neutral particles pass through an ionization source (C1) that ionizes the particles (Modi et al., 2003). The ionized particles cross an electronic gate (C2) that provides the START of the ToF (example of such time tagging characterization is given in Brock et al. 2000). Then the particles are accelerated up to more than 1 keV and deflected by an electrostatic system (C3) and are detected by a STOP MCP detector (C4). The ToF provides information about mass (since the spread in energy is assumed to be negligible).
For detecting particles between 0.02–1 keV, the neutrals pass through a double grating system (with slits of nanometric dimension) (D1) (Orsini et al. 2009b) that provides photon suppression. A shuttering system allows to move the two gratings one with respect to the other in order to permit the neutrals to enter in the sensor only when the slits are aligned (open gate), which defines the START time. Then the neutrals fly into a ToF chamber and are converted into ions by using the technique of neutral-ion conversion surface (D2) (Wurz, 2000). The ionization efficiency is sufficient at the lowest particle energies and even increases for higher energies. When particles impact at the conversion surface electrons are released, even at low impact energies (Wieser et al., 2005). An electrostatic system accelerates the released electrons keeping them well aligned to the original projection to the surface impacting point and pushing them toward the MCP detector, which also has position sensing capability (D3). The MCP will provide the STOP signal for the ToF measurement as well as the angular direction of the velocity of the registered neutral particle. The atom converted in ion by the conversion surface will be accelerated and detected by a MCP (D4) that will provide an additional STOP signal. Moreover, for increasing the geometrical factor, the detector can be used in open-gate mode. In this way the ToF can be identified using as START the first MCP signal. However, the energy resolution will be lower, due to the indetermination in the energy and recoil angle after the impact on the conversion surface.

The FOV of the two detection systems is 5°×30°. The higher energy distribution will be analyzed with an angular resolution of 5°x2.5° (high angular resolution mode) or 5°x5° (low angular resolution mode).

Taking into account the instrument elements, the estimate of the high energy detector geometrical factor is in the range 4 10^{-4}-2 10^{-5} cm^2 sr, and the mass spectrometer efficiency of about 0.14 (counts/s)/cm^{-3}.

These sensor characteristics permit a detection of the estimated particle release. In fact, if the estimated particle flux due to IS from NEO is 10^7 cm^{-2} s^{-1}, more than 1200 counts are estimated in the high energy sensor for 1 minute of integration time. The estimated gas density is, at least, of the order of 10^2 cm^{-3} close to the surface. In this case, for a 1-minute integration time, about 1000 counts in the low energy sensor are expected.

All the NPA operations will be controlled by an FPGA based microcontroller (Sensor Control Unit - SCU).

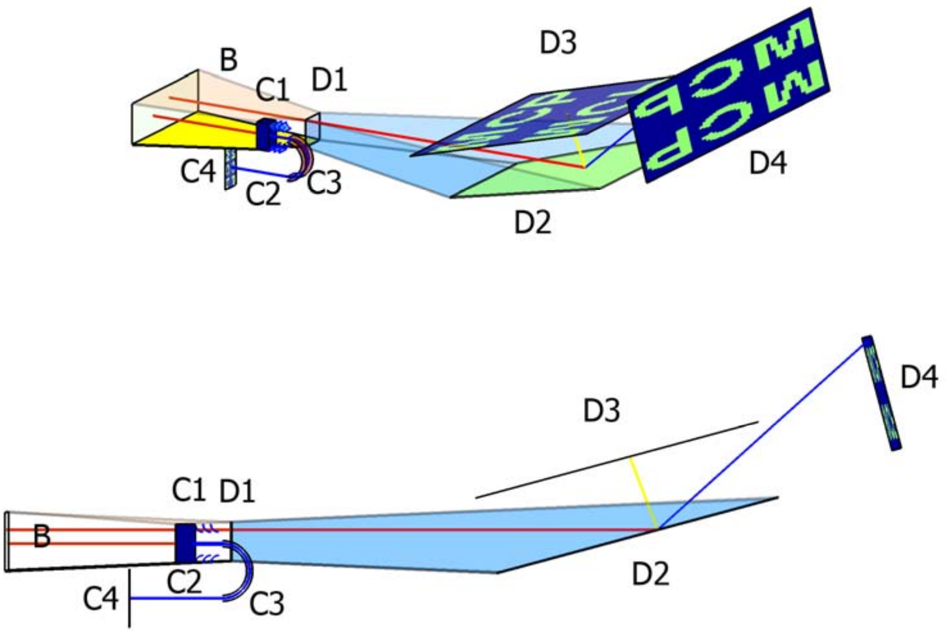

Figure 18. NPA basic concept

In summary the NPA sensor consists of the following subsystems:

- A: Cover (not shown); B: Parallel plate collimator, balanced biased +5kV –5kV;
- Mass spectrometer: C1: ionizing source, C2: electronic gate, C3: ESA, C4: MCP, C5: 2D Anode system (not shown).
- The particle (red line) enters from the left side (B), gets ionized (blue line) passing through C1, accelerated by C2, deflected by C3, and finally detected by C4.
- High energy detector: D1 two nanogrids and the shuttering system, D2: Conversion Surface; D3 MCP electron detector; D4: MCP ion detector; D5: 2D Anode system (not shown).

- The particle (red line) enters from the left side (B), passes through D1, hits D2, releasing electrons (yellow line) detected by D3. The particle is deviated and ionized (blue line). Finally, the ion is detected by D4.

Table 19 Mass spectrometer geometrical factor

Element	Value	Unit
Cross section	$1.4\ 10^{-16}$	cm^2
Ionization lenght	2	cm
Electron current	$6.2\ 10^{15}$	$e^-/s=1$ mA
Collection efficiency	0.1	
TOTAL	**0.14**	**(Cnt/s)/cm^{-3}**

Table 20 High energy detector geometrical factor

Element	Value	Unit
FOV (5°x30°)	0.04	sr
Aperture	1	cm^2
Geometrical aperture ratio	0.2	
Shuttering grid	0.1	
Conversion surface efficiency (energy dependent)	0.001-0.1	
MCP electron efficiency	0.9	
MCP ion efficiency	0.5	
TOTAL	**$4\ 10^{-4}$-$2\ 10^{-5}$**	**cm^2 sr**

8.8.3.3 Orbit, operations and pointing requirements

The preferred satellite path is a 3D-axis-stabilized orbit at few kilometers above a NEO of radius less than 1 km. `
The pointing requirement is to have the object within the 30°x5° FOV of the instrument and to know the position and the orientation of the spacecraft with an accuracy of 10 mrad.
The orbit has not to be circular around the target as it may be inferred from the simulation parameters. Also during the close-approach phases the instrument should be active.
The thrusters-emitted gas may significantly affect measurements during specific time periods. For this reason, NPA must be located far from the thrusters.
The instrument should be operated in survey mode during the first approaches to the target. Given the estimated signal, the first measurements should be performed at distances below 3 km from the object surface. While the mass spectrometer should be operated in the illuminated and not illuminated sides, the high energy detector needs to perform observation in the sun-illuminated side. Simultaneous measurements of the two sensors are necessary. Crucial measurements are required during the closest approach phase.
Hence, according to the present mission scenario,

- calibration and survey operations are requested during phase “Far 1” (at least 10 hours);

- survey operations for high energy sensor (24 hours) and for mass spectrometer (at least 48 hours) are requested during phase "gravity field 2" ;
- nominal science operations are requested for achieving the primary scientific objectives during orbital phase "near 3", especially in the illuminated side. The average erosion rate can be evaluated with a statistics of at least 10 days of illuminated-side observations, but continuous day-side observations are requested for the study of erosion as a function of solar wind conditions especially for the high energy detector (estimation of about 30 days). Further observations time (at least 5 days) in survey mode is needed for the mass spectrometer in the night side.
- Nominal science operations in the descent phase, when the spacecraft is closer to the target (estimation 10 h).

A rough estimation of the total data volume during the mission is about 100 Mbytes for simple compression.

Table 21 Operation modes of the NPA (see next section)

	Calibration	survey		nominal	
Unit		Mass spectr.	SCU+High energy detector	Mass spectr.	SCU+High energy detector
Duration	10h	48h+120h	24h	720h+10h	720h+10h
Power (peak and mean)	7 W	1.5 W	3+7 W	1.5 W	3+7 W
Pointing requirements		0.1 deg/s	0.1 deg/s	0.1 deg/s	0.1 deg/s
No-compressed Telemetry (Data Rate & Volume)	770 Bytes/s	3 Bytes/s	3 Bytes/s	7 Bytes/s	51 Bytes/s
Operational constraints	Far from sources (cruise phase)		Illuminated side	Mainly illuminated side	Illuminated side
Number of occurrence of the operation					

8.8.3.4 Interfaces and physical resource requirements

The spacecraft resources for this instrument are not demanding. In fact, the dimension of the whole NPA instrument is about 20x20x10 cm^3, its mass will be about 2 kg and the total power requirement is about 11 W.

Table 22: Summary of NPA resources

	Mass (kg)	**Power (W)**	**Volume (cm^3)**	**Data rate (bytes/s)**
Mass spectrometer	1	1.5	15x10x10	7
High energy detector	1	7	20x10x10	51
SCU	0.2	3	16x1x10	N/A
NPA TOT	**2.2**	**11.5**	20x20x10	58

The required telemetry resources are not expensive. For the nominal science mode, if we consider 50 mass channels the mass spectrometer requires about 50x2 bytes/s, corresponding to 7 bytes/s for an integration time of 15 s. If we consider 32 TOF channels and 12 angular directions and 2 MCP signals the high-energy detection requires about 770 bytes/s, corresponding to 51 bytes/s for an integration time of 15 s.
In a survey mode, the foreseen telemetry rate is about half for the mass spectrometer (3 bytes/s) and 16 TOF x 3 angular dir. x 2 MCPs / 30s =3 bytes/s.
Data compression is provided by an included high reliability computation unit: factor 2 (Semi-log only), factor 3 loss-less (Semi-log + HArtmann-Quad-tree loss less) and 4.5 lossy (Semi-log + HArtmann-Quad-tree lossy). The SCU (System Control Unit) collects and processes all instrument data. The data inter face is CAN bus compatible.
The instrument design includes a DC/DC converter (28 V, regulated, from spacecraft) to feed the instrument with the required low voltage lines.

The instrument has no specific thermal control requirements.
There is no sun avoidance requirement.
The operational temperature is between -20°C to +40°C., non operational between -40°C to +50°C. The Switch-On-Temperature is min. -30°C and max +40°C.

8.8.3.5 Calibration

Far from sources, during cruise phase, it is requested a functional test of the instrument in order to verify the readout noise threshold.

8.8.3.6 Cleanliness, planetary protection and pre-launch activities

The instrument (MCPs) requires purging and humidity monitoring up to launch.

8.8.3.7 Critical points

The sensors are adequate for environments requiring strong radiation shielding like the BepiColombo mission to Mercury. The environment and mission duration of MarcoPolo is less constraining in comparison.
The UV and IR noise should be better evaluated. Anyway, the grids at the entrance prevents UV noise; an IR filter could be added in the case IR radiation will not be negligible.

8.8.3.8 Heritage

ENA sensors already flown, in the energy range tens eV and few keV, are IMAGE/LENA, MEX/ARPERA-3/NPD, VEX/ARPERA-4/NPD, Chandrayaan-one/CENA, IBEX-Hi. The present concept is based on the SERENA-ELENA design (Orsini et al. 2009b), developed at INAF-IFSI, to be on board BepiColombo/MPO because of its better angular resolution and UV noise suppression.
Many mass spectrometers have been flown in past space planetary missions. The proposed design is based on the heritage of BepiColombo/SERENA-STROFIO (Orsini et al. 2009a), developed and optimized for detection of very tenuous gas environment. More specifically, the ionization source is based on the heritage of STROFIO, the electronic gating system on BepiColombo/SERENA-PICAM (Orsini et al. 2009a), while electrostatic analyzers have been extensively studied in the frame of the CLUSTER/CIS instrument (Di Lellis et al. 1993; Rème et al., 1997). Presently a prototype is been tested at Southwest Research Institute for applications on the BepiColombo spacecraft to Mercury and the Ladee mission to the Moon.

8.8.3.9 References

Brock, A,. N. Rodriguez,and R.N. Zare, 2000. Characterization of a Hadamard Time-of-Fligth spectrometer, Rev. of Sci. Inst., **71**, 1306-1318.

Brown et al.: *The Fall, Recovery, Orbit, and Composition of the Tagish Lake Meteorite: A New Type of Carbonaceous Chondrite*, Science, 290, 2000.

Di Lellis, A.M., P. Baldetti G. Chionchio, V. Formisano, 1993. The Hot ion analyzer instrument for the ESA Cluster mission; Il Nuovo Cimento -**16C**, N. 6 10 Novembre-Dicembre.

Hapke, B., *Space weathering from Mercury to the asteroid belt*, J. Geophys. Res., **106**, 10039-10074, 2001.

Hapke, B.W., Cassidy, W.A.: *Is the moon really as smooth as billiard ball/ remarks concerning recent models of sputtering on the lunar surface*, Geophys. Res. Lett. **5**, 297-300, 1978.

Hofer, W. O.: Angular, Energy and Mass Distribution of Sputtered Particles, Sputtering by particle Bombardment III, Eds: R. Behrisch, K. Wittmaack, Springer-Verlag Berlin Heidemberg 1991

Jurac, S., Johnson, R.E., Richardson, J.D., Paranicas, C.: *Satellite sputtering in Saturn's magnetosphere*, Plan. And Sp. Sci., **49**, 319-326, 2001.

Milillo, A., S. Orsini, P. Wurz, D. Delcourt, E. Kallio, R.M. Killen, H. Lammer, S. Massetti, A. Mura, S. Barabash, G. Cremonese, I.A. Daglis, E. De Angelis, A.M. Di Lellis, S. Livi, V. Mangano, K. Torkar, *Surface-Exosphere-Magnetosphere System of Mercury,* Space Science Reviews, **117**, issue 3, 397-444, 2005.

Modi A., N. Koratkar, E. Lass, B. Wei and P. M. Ajayan, 2003. Miniaturized gas ionization sensors using carbon nanotubes, Nature **424**, 171-174, doi:10.1038/nature01777.

Mura, A., S. Orsini, A. Milillo, D. Delcourt S. Massetti and E. De Angelis, *Dayside H+ circulation at Mercury and neutral particle emission*, Icarus, **175**, 305, 2005

Orsini, S., S. Livi, K. Torkar, S. Barabash, A. Milillo, P. Wurz, A. M. Di Lellis, E. Kallio and the SERENA team, *SERENA:a suite of four instruments (ELENA, STROFIO, PICAM and MIPA) on board BepiColombo-MPO for particle detection in the Hermean Environment*, BepiColombo Special Issue on Planetary and Space Science, in press, 2009a

Orsini, S., A.M. Di Lellis, A. Milillo, E. De Angelis, A. Mura, S. Selci, R. Leoni, F. Mattioli, S. Massetti, R. Orfei, I. Dandouras, P. Cerulli-Irelli, N. Vertolli, *Low energy high angular resolution neutral atom detection by means of micro-shuttering techniques: the BepiColombo SERENA/ELENA sensor*, proceeding of the meeting "Future perspective of space plasma and instrumentation and international collaboration" (Rikkyo University, Tokyo, Japan, November 1-3 2006), 2009b (arXiv: 0811.4722)

Plainaki, C., A. Milillo, S. Orsini, A. Mura, E. De Angelis, A. M. Di Lellis, E. Dotto, S. Livi, V. Mangano, S. Massetti, M. E. Palumbo, *Space Weathering on Near Earth Objects based on neutral particle detection*, Planetary and Space Science, **57**, 384–392 2009 Rème, H., J.-M. Bosqued and J.A. Sauvaud *et al.*, 1997. The cluster ion spectrometry (CIS) experiment, *Space Sci. Rev.* **79**, 303–350.

Sigmund, P. (1969) *Theory of sputtering. I. Sputtering yield of amorphous and polycrystalline targets*. Phys. Rev. **184**, 383–416.
Sieveka, E.M., R.E. Johnson, (1984) *Ejection of atoms and molecules from Io by plasma-ion impact*, Astrophys. Journal, **287**, 418-426.
Wieser, M., P. Wurz, R.J. Nemanich, and S.A. Fuselier., 2005. Secondary electron emission of CVD diamond by impact of slow H+, D+, H2+, C+, O+, and O2+ ions, Jou. Appl. Phys. **98**, 034906-1 - 034906-4.

8.8.3.10 Summary table

Table 23 Summary data sheet of the NPA

Parameter	**Units**	**Value/Description**	**Remarks**
Reference P/L	N/A	Serena on BepiC	
Type of Ion supressor		electrostatic lens	
Type of ionisation		Carbon nanotubes	
Type of detector		MCP	
Type of positioning system			
Geometrical Factory mass spectrometer			
Equivalent aperture	mm^2	50	
FOV	°x°	5x30 deg	
Angular resolution	°x°		
Number of mass channels	#	50	
Dynamic range	$(Cnt/s)/cm^{-3}$	0.14	
Energy range	eV	<10	
Mass resolution	AMU	50	
Sensitivity			
Geometrical Factory			
Equivalent aperture	mm^2	100	
FOV	°x°	5x30 deg	
Angular resolution	°x°	5x2.5	
Number of channels	#	12	
Overall geom. factor	cm^2*sr	$4\ 10^{-4}$-$2\ 10^{-5}$	
Energy range	eV	10-1000	
Spectral or energy resolution		32 TOF	
Sensitivity			
Detector			
Active area			

Acquisition time			
Orbit			
Pointing	n/a	Toward target	
Type of orbit	n/a	Below few km distance from NEO	
PHYSICAL			
Mass, total	kg	2.2	
Dimension	cm^3	20x20x10	
No. of units	#	1	
Footprint	mm		
POWER			
Total average power	W	11.5	
Peak power	W	11.5	
Data rate / volume			
data rate	kbs	0.5	
Compression	n/a	2	internally done
Total data	Gbit	1.44 Gbit	
Thermal			
Operating temperature	°C	-20 to +40	
Non ops temperature	°C	-40 to +50	
Contamination			
Particulate/chemical	n/a		requires purging and humidity monitoring up to launch.

9 DESCRIPTION OF COMPLEMENTARY INSTRUMENTS

9.1 Laser altimeter

The laser altimeter remains as an optional instrument on the orbiter

9.1.1 Introduction

A Laser altimeter will contribute to the characterization of the target asteroid in the areas of geodesy and geophysics, and will also be crucial for the navigation of the spacecraft in the gravity field of the asteroid by providing accurate range data to the asteroid.

9.1.2 Scientific Goals and Performance Requirements

The following requirements are cited from the Science Requirements Document as reference for the expected scientific performance of this instrument;
GR-030: A shape model of the NEO shall be obtained with an accuracy of typically 1 m in height and spatial resolution with respect to the centre of mass, in both illuminated and unilluminated regions.
GR-040: The mass of the NEO shall be determined to an accuracy of about 1%.
AS-020: The J2 terms of the gravitational field should be determined with an accuracy of 10%.

The following list describes the expected output values and contributions to other complex scientific and engineering aspects:

- Derive topographic profiles
- Derive a global shape model of the target asteroid
- Assist in studies of asteroid geodetic parameters (e.g., coordinate system, rotation)
- Assist in orbit determination and gravity data modeling
- Assist in spacecraft manoeuvring
- Measure surface roughness and albedo (at the laser wavelength)

Performance;

- High signal-to-noise for reliable pulse detection (>95%) during night and day from a typical range of 5 km. Minimum range: 100 m.
- Range accuracy: < 0.5 m
- Laser footprint from 5 km: 1 m (tbd.). Divergence (full cone): 20 mrad
- Pulse repetition rate shall allow for a seamless along-track ground pattern
- Allow for pulse shape modeling

Lifetime: 1 year; total no of shots: 5 Mio (classical system, tbc.)
(see performance spread sheet in Table 24)

9.1.3 Description

The instrument will consist essentially of 3 components, a Laser transmitter, a Laser receiver with a receiver optics of approx. 2 cm, as well as a data processing unit.

9.1.3.1 Instrument concept

The instrument will measure the two-way travel time of a Laser pulse travelling from the instrument to the surface and back. A topographic profile along the ground track of the spacecraft will be produced. By interpolation, a global shape model will be derived. By measurements of pulse amplitude and shape, the reflectivity of the surface, as well as slope and surface roughness (within the footprint of the Laser) can be modelled.
Two design options can be considered (chapter 9.1.3.7)

A topographic profile along the ground track of the spacecraft will be produced. As an option, we envisage a mechanical scanning mechanism to increase the instrument field-of-view perpendicular the spacecraft track.
The scanner is a rotating circular wedge prism, which sits in front of a combined Tx-Rx optics. The free aperture of this scanner is 4 cm resp 2.5 cm (see Table 1), the rotation speed is low.
In Figure 19, the ground pattern of such a scanner is depicted in principle. The labelling of the axes in terms of scale is not representative for a potential Marco Polo scanner. The rotating speed of the scanner will be adapted to the range and speed over ground of the Marco Polo spacecraft. The blue squares represent the positions of the FOV of the detector and the laser spot for each laser pulse.

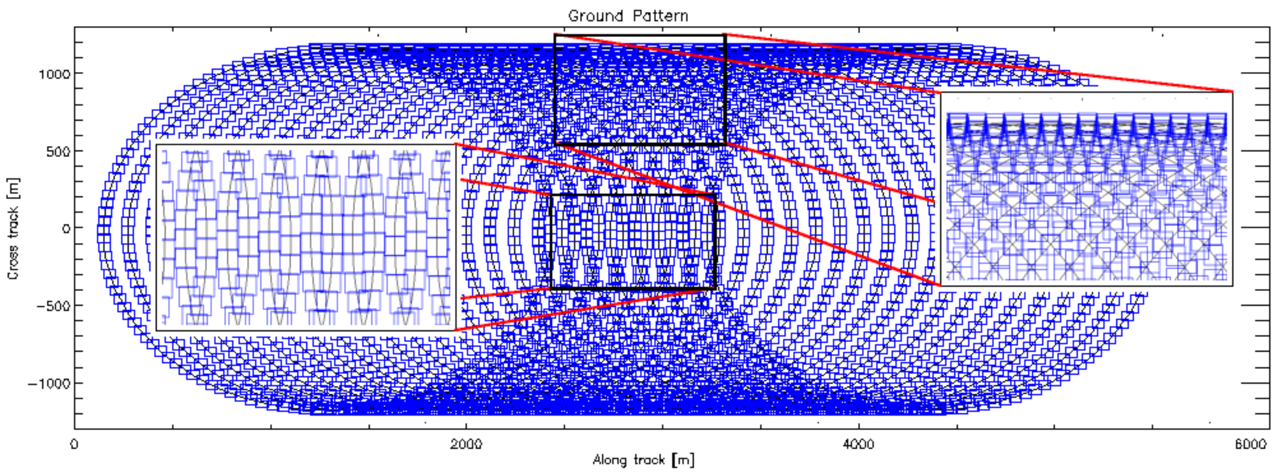

Figure 19: Ground pattern of scanner consisting of one rotating wedge prism (scale not representative for Marco Polo)

Figure 20 explains the working principle and optical path of a combined Tx-Rx optics including scanner. The laser beam is depicted in red, the path of the light reflected from the surface in blue. The laser beam becomes expanded by two lenses and deviated by the wedge prism. The path of reflected light is the same as for the laser beam expect for a mirror which feds the reflected light to the detector.

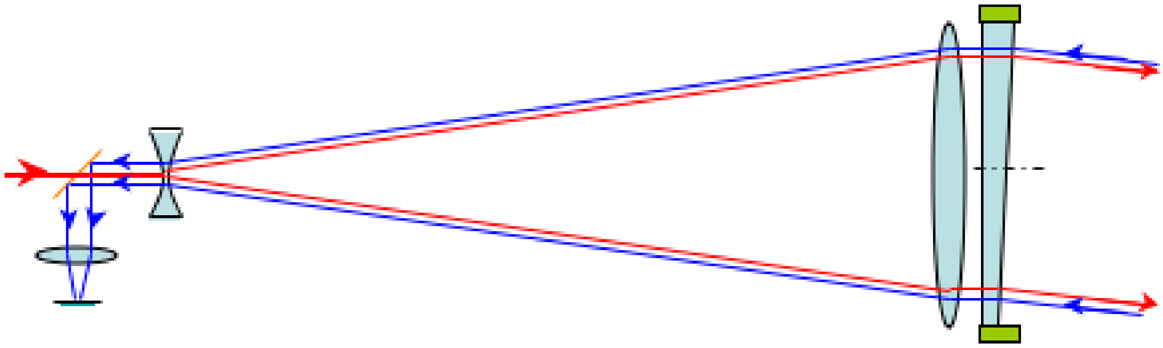

Figure 20 Optical path of a combined Tx-Rx optics. The wedge prims is depicted at the right.

The operational and technical details of the scanner are under investigation.

9.1.3.2 Orbit, operations and pointing requirements

The instrument will operate during approach to the asteroid and during the spacecraft orbit phase. It will typically fire at a rate of 1 Hz, which ensures a seamless ground pattern in along-track direction.

Nighttime observations and daytime observations (which have to overcome the solar background noise) are equally possible. The pointing shall be accurate to within the size of the Laser footprint. The instrument should also be capable for 2-way (offline) ranging measurements to terrestrial Laser stations for instrument alignment calibration, performance tests, and also, to support the tracking of the spacecraft.

The divergence of the laser beam is 200 µrad, which results in a laser spot diameter of 1 m at a range of 5 km. At lower ranges, the footprint decreases below 1 m and the pulse repetition rate will be increased in order to obtain the seamless along-track spacing, which results in a finer grid spacing, e. g. 0.1 m from 1 km range.

9.1.3.3 Interfaces and physical resource requirements

- Instrument size of 23 x 16 x 14 cm
- Total mass not exceeding 5 kg (incl. DPU)
- Thermal control interface (e. g. heat pipe to radiator or direct radiation to space)
- Temperature ranges:

Operational:
Electronic boxes: -20°C to +50°C
Laser head, Detector: -10°C to +45°C
Non-Operational:
Electronic boxes: -40°C to +60°C
Laser head, Detector: -40°C to +60°C

9.1.3.4 Calibration

- Verification of the alignment of transmitter and receiver using Earth ranging, which requires an unobstructed FOV during the cruise phase to the asteroid (no aperture covers, no masking by other s/c components)
- Measurements of instrument alignment wrt the spacecraft coordinate system, in particular the camera using star observations
- Radiometric calibration of the Laser receiver using star observations

9.1.3.5 Cleanliness, planetary protection and pre-launch activities

Cleanliness and Contamination Control during instrument and spacecraft AIV according to the very strict rules for space-laser applications. A contamination budget of level 500A/2 until end of mission for optical surfaces exposed to space or the asteroids surface is required. The amount of contamination caused by landing and sampling (raised dust) shall be estimated by the S/C and the potential impact on the laser altimeter optics considered.

Planetary Protection: no special requirements from the laser altimeter

9.1.3.6 TRL and development plan

The following TRLs (NASA Technology Readiness Levels) are mainly derived from the current BELA development for BepiColombo mission. Once the BELA development is finished, the TRL is 9.

- Laser Optics/Optomechanic/BEX: TRL 6
- Laser Electronics: TRL 6
- Laser Pump diodes: TRL 6

Thermal-vacuum, vibration and EMC tests were conducted with all laser subsystems.
The pump diode qualification program was directly contracted with ESA. A comprehensive test program is ongoing. For BELA, the laser pump diodes are not seen as the most vulnerable point.

- Baffles: TRL 6

A reflective Stavroudis-Baffle is used for the Receiver (20 cm diameter) and for the transmitter (9 cm diameter). Other baffle types were studied at DLR and ESA contracted two Baffle studies for the BepiColombo program.
In the frame of the development of a transmitter baffle for BELA, DLR studied, modelled and designed several baffle types. Only minor problem for the adaption of the baffles for the requirements of the MarcoPolo mission.

- Rx Telescope: TRL 6

Prototype fabricated, several tests for performance verification

- Detector and Focal Plane Assembly: TRL 6

Start/Rangefinder Electronics incl. Algorithm (Filter, Pulse shape analysis etc): TRL 4
Bread Board of a fast start electronic tested at DLR
Bread Board of a rangefinder electronic tested at UBE

Rangefinder combined with start electronic under development (detailed design phase)

Schematic BELA hardware configuration (see Figure 21):
The laser electronic boxes (Laser Electronics, Electronic Unit) are separated from the optical bench of the instrument. The Electronic Unit holds the power converter, the digital processing unit and the rangefinder electronic.
The Laser Electronics controls the laser operation and drives the pump diodes inside the laser head in which the laser beam is generated. The laser beam becomes collimated and expanded by the beam expander, exits the instrument through the transmitter baffle and hits the asteroid surface.
The reflected signal is received and focussed on the detector assembly. The rangefinder inside the Electronics Unit analyzes the return signal.
The baffles protect the transmitter and receiver optics against environmental fluxes (mostly
Sun).
Electrical and optical harness is not shown in the Figure 21.

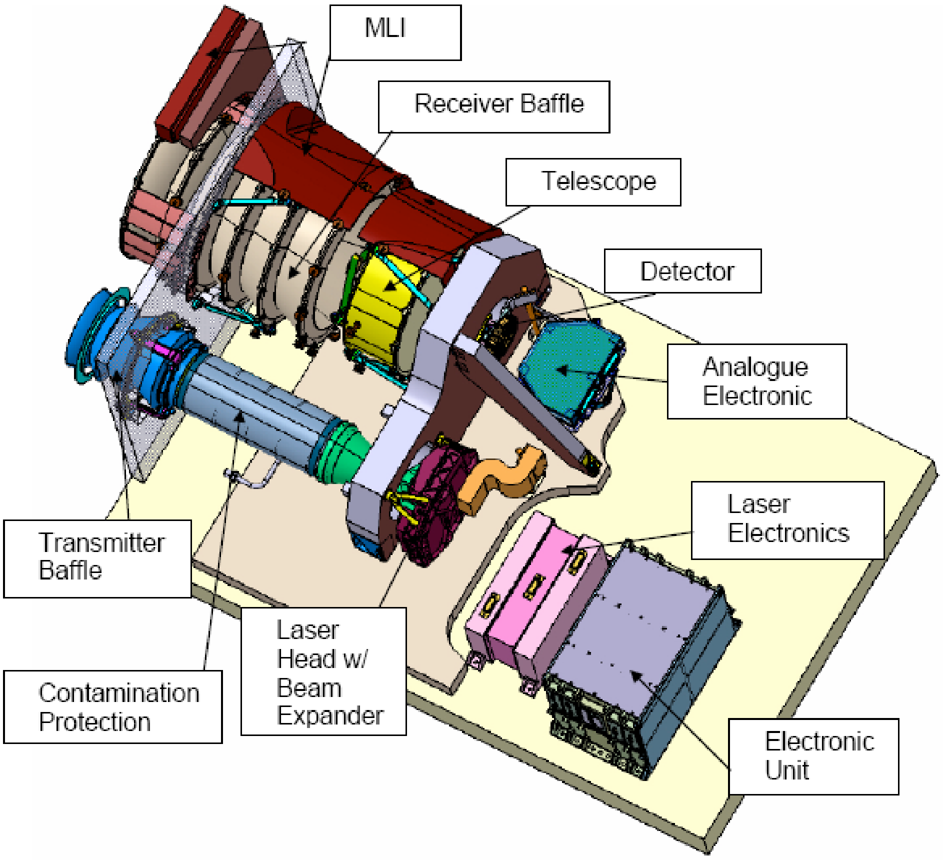

Figure 21 Sketchmap of the BELA laser altimeter

The laser box comprises of two laser lines in cold-redundancy configuration. The same applies to the laser electronics, the digital processing unit and the power converters.

9.1.3.7 Critical points and heritage

As optical receiver systems are standard for space applications, the proper choice of the optical system is not critical. In contrast, the choice of an appropriate laser drives the complexity of the instrument.

The Marco Polo Laser Altimeter bases on the BELA (BepiColombo Laser Altimeter) wherever possible. On the one side, experiences and knowledge gathered during the BELA programme will be available for the Marco Polo Laser Altimeter. On the other side, hardware used for BELA will be widely used for the Marco Polo Laser Altimeter. This is mostly relevant for parts, which are dedicated laser altimeter parts like optical elements, optical coatings, laser pump diode technology, laser driver electronics, detector electronic & algorithms and much more. All these parts and sub-assemblies are successfully space-qualified during the BELA program. Of course, BELA differs much from the Marco Polo Laser Altimeter in terms of performance and operation requirements, but the basic principle is the same and requires the same laser hardware parts, laboratories, procedures, ground support equipment etc. which all is established and used during the BELA program. Therefore, the difference between BELA and the Marco Polo Laser Altimeter is not a drawback.

Two different instrument configurations are considered:

“MARCO I” is a classical laser altimeter like BELA with performance parameters specifically designed for the mission. This would reduce size, total mass, and required power compared to BELA. We therefore do not anticipate any major changes to the detector and onboard-software etc.

“MARCO II” is al laser altimeter based on single-photon counting. The detector is a silicon APD, operated as photon-counting device, which requires only a few (< 10) signal photons for a detection event and consequently a very small laser. Such Laser systems now become operational in terrestrial airborne applications, and have been studied by a DLR-lead consortium under ESA contract in 2002: LAPE: Laser Altimeter for Planetary Exploration. Such a new system would have dramatically reduced size, mass, and power requirements. However, besides the development and space-qualification of the detector, a new pulse detection and processing scheme must be developed.

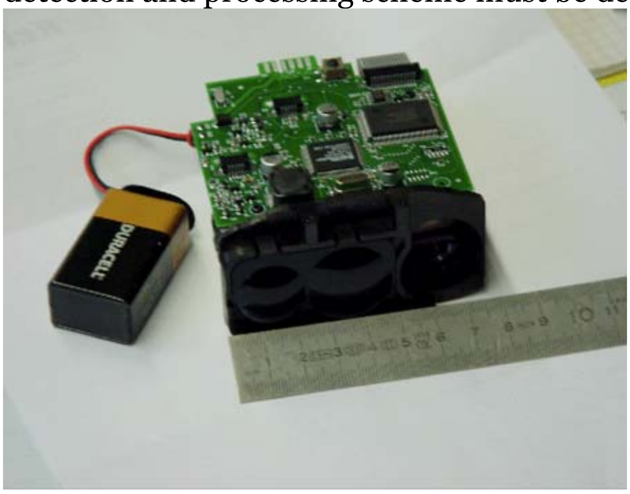

Figure 22 Microchip laser

9.1.3.8 Summary table

Table 24 Summary of laser altimeter parameters and instrument performance

	MARCO I Classical Laser Altimeter	**MARCO II Single-Photon Counting Laser Altimeter**
Performance Parameter		
Laser	4 mJ	0.1 mJ
Laser Wavelength	1064 nm	1064 nm
Laser Pulse Length	3-8 ns	1-10 fs
Pulse Repetition Rate **)	1 Hz	1 Hz
Laser Beam Divergence	200 µrad (tbc.)	200 µrad (tbc.)
Laser Spot on surface (at 5 km range)	1m	1m
Receiver Optics Diameter	4 cm	2.5 cm
Detector Quantum Efficiency	0.25	0.25
Max. range to surface ***)	5 km	5 km
Optical system transmission	0.8	0.8
Albedo	0.05	0.05
Length of Range Gate	200 ns	200 ns
Bandwith of Rx optical filter	1.0 nm	1.0 nm
Signal Photo Electrons	1100	10
Instrument Parameter		
Operation Power *)	22 W	22 W
Data rate	800 bit/s (80 per shot)*	tbd
Dimensions	15 x 10 x 10 cm (tbc)	10 x 5 x 5 cm (tbc)
Nominal Lifetime	1 year or 5 Mio pulses	1 year or 5 pulses
Total Mass	4 kg (tbc.)	3.5 kg (tbc.)

*) Primary power from S/C. The instrument provides its own power converters with 75% efficiency. The difference in pulse energy has no remarkable impact on the overall instrument power.
**) The given value is the nominal value. The pulse repetition rate can be adjusted in order to fulfil scientific requirements
***) The maximum range results from the MarcoPolo CDF study. A larger range is possible.

9.2 Optional lander element and payloads

The lander forms and optional package that can accommodate a large variety of possible payload instruments. It can be only included if sufficient resources are available from the main S/C not compromising the main goal of the mission to return surface material to Earth.

The overall lander concept is based on a low resource approach. Table 25 summarizes the lander main subsystems and provides a mass breakdown.

Table 25 Lander mass breakdown (reproduced from MarcoPolo-R proposal)

Element	**Mass [kg]**
Structure	2.9
Thermal control	0.4
Mobility mechanism	0.4
Communication	0.4
Command and Data	0.5
Power (incl. battery)	1.0
Payload	3.0
Margin (20%)	1.7
Total	10.3

The following suite of scientific instruments is suggested as a possible payload package:

- Camera 0.4 kg
- LIBS 1.2 kg
- Vis/IR microscope 0.7 kg
- Radar tomographer 0.7 kg
- Thermal Probe 0.2 kg

The radar tomographer is a bi-static radar and requires another element of 1.2 kg on the orbiter.